# Generic Mott-Hubbard phase diagram for extended Hubbard models without Umklapp scattering

Florian Gebhard [*] and Kevin Bauerbach
*Fachbereich Physik, Philipps-Universität Marburg, 35032 Marburg, Germany*

Örs Legeza [†]
*Fachbereich Physik, Philipps-Universität Marburg, 35032 Marburg, Germany;*
*Strongly Correlated Systems Lendület Research Group, Institute for Solid State Physics and Optics,*
*HUN-REN Wigner Research Centre for Physics, P.O. Box 49, 1525 Budapest, Hungary;*
*and Institute for Advanced Study, Technical University of Munich, Lichtenbergstraße 2a, 85748 Garching, Germany*

(Received 9 September 2023; revised 31 October 2023; accepted 1 November 2023; published 15 November 2023)

We determine the ground-state phase diagram for the $1/r$-Hubbard model with repulsive nearest-neighbor interaction at half band filling using the density-matrix renormalization group method. Due to the absence of Umklapp scattering, the phase diagram displays finite regions for the three generic phases, namely, a Luttinger liquid metal for weak interactions, a Mott-Hubbard insulator for dominant Hubbard interactions, and a charge-density-wave insulator for dominant nearest-neighbor interactions. Up to moderate interaction strengths, the quantum phase transitions between the metallic and insulating phases are continuous, i.e., the gap opens continuously as a function of the interaction strength. We conclude that generic short-range interactions do not change the nature of the Mott transition qualitatively.

DOI: 10.1103/PhysRevB.108.205130

## I. OVERVIEW

After a short introduction in Sec. I A, we present in Sec. I B the generic Mott-Hubbard phase diagram for extended Hubbard models without Umklapp scattering, the central result of our work. The corresponding model and its ground-state properties are discussed in the remainder of this paper, as outlined in Sec. I C.

### A. Introduction

The Mott transition is one of the long-standing problems in condensed-matter many-body physics [1–3]. As formalized in the Hubbard model [4–6], an electronic system with a single band of width $W$ and a purely local interaction of strength $U$ will be a metal for weak interactions, $W \ll U$, and an insulator for strong interactions, $U \gg W$. As argued by Mott early on [7], there must be a metal-to-insulator transition, generically at $U_c \approx W$ when the two energy scales are comparable, irrespective of magnetic or charge order.

The quantitative analysis of a quantum phase transition in an interacting many-particle system is notoriously difficult. Concomitantly, analytical solutions are scarce even for the simplest models and in one spatial dimension [2,8,9]. Numerical approaches in finite dimensions are hampered by finite-size effects, so that the calculation of ground-state quantities is also best performed for one-dimensional model systems. In one dimension, the numerical density-matrix renormalization group (DMRG) method provides accurate data for large enough systems with of the order of a hundred lattice sites and particles [10–14].

In some respects, one-dimensional systems behave qualitatively differently from their three-dimensional counterparts. Most importantly, they generically display the perfect-nesting instability because the two Fermi points at half band filling are connected by half a reciprocal lattice vector. Umklapp scattering turns the system into an insulating one as soon as the (effective) interaction of the particles becomes finite [15]. Therefore $U_c = 0^+$ is the generic situation [2,8,9], in contrast to Mott's expectations. Correspondingly, the phase diagram for the one-dimensional Hubbard model does not contain a finite metallic region. When the Hubbard model is extended by the inclusion of a nearest-neighbor interaction, the ground-state phase diagram becomes more varied, but one can only study quantum phase transitions between Mott-Hubbard, charge-density-wave (CDW) insulator, and bond-order-wave (BOW) insulator phases [16–18]. For more information on density waves in strongly correlated quantum chains, see Ref. [19].

To avoid Umklapp scattering at weak coupling, one can investigate models with only right-moving electrons that display only one Fermi point. A known example is the $1/r$-Hubbard model with its linear dispersion relation within the Brillouin zone [2,20,21]. Indeed, as indicated analytically [20,22] and recently corroborated using the DMRG method [23], the critical interaction strength for the Mott transition is finite in the $1/r$-Hubbard model.

Therefore we can study the competition of the metallic and insulating phases and the corresponding quantum phase transitions using the extended $1/r$-Hubbard model in one

[*] florian.gebhard@physik.uni-marburg.de
[†] legeza.ors@wigner.hu

 

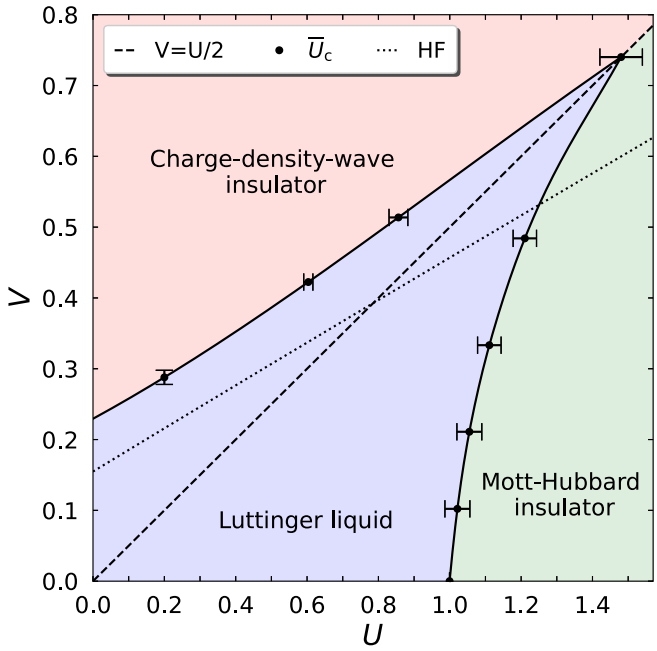


FIG. 1. Phase diagram of the one-dimensional extended $1/r$-Hubbard model; energies are in units of the bandwidth, $W = 1$. Solid circles, estimates for the critical interaction, $\bar{U}_c$, with error bounds; solid curves, spline interpolations through the solid circles as guides to the eye; dotted line, Hartree-Fock (HF) result for the transition between metal and charge-density-wave insulator.

dimension. The resulting phase diagram should be generic in the sense that each phase covers a finite region in the ground-state phase diagram, as is expected for a three-dimensional system ($d = 3$) at half band filling without Umklapp scattering.

We shall argue that for the extended $1/r$-Hubbard model the transitions between metallic and insulating phases are continuous in the sense that the gap opens continuously as a function of the interaction parameters. However, in the limit of high spatial dimensions, $d \to \infty$, quantum Monte Carlo (QMC) simulations for the dynamical mean-field theory problem indicate that the Mott transition is discontinuous even for the bare Hubbard model: The preformed gap for $U > U_{c,1}$ becomes visible when the quasiparticle peak in the metallic phase vanishes at $U_{c,2} > U_{c,1}$ [24]. It remains to be clarified whether the Mott transition in the Hubbard model is generically continuous or discontinuous in finite dimensions larger than one dimension.

### B. Phase diagram

The phase diagram in Fig. 1 depicts the central result of our work. It shows the generic Mott-Hubbard phase diagram for extended Hubbard models without Umklapp scattering. Derived for the special case of the extended $1/r$-Hubbard model, the phase diagram displays finite regions for the generic phases of an interacting electron system with a single half-filled band of width $W \equiv 1$ and with tunable local interaction $U$ and nearest-neighbor interaction $V$.

As can be argued using weak-coupling and strong-coupling perturbation theory, there should be a metallic phase at weak interactions, $U, V \ll W$, that becomes unstable, turning into a Mott-Hubbard insulator for dominant Hubbard interaction, $U \gg V, W$, or turning into a charge-density-wave (CDW) insulator for dominant nearest-neighbor interactions, $V \gg U, W$. The critical interactions for the corresponding quantum phase transitions should be finite, the competing interactions being of the same order of magnitude.

Indeed, when the Coulomb interactions are dominant, $U, V \gg W$, the separation line between the Mott-Hubbard insulator and the CDW insulator should be $V = U/2$. The corresponding line is included as a dashed line in Fig. 1. For large $U, V$, we find $V_c(U) \gtrsim U/2$, with small deviations in favor of the Mott-Hubbard insulator. For this reason, we only show the phase diagram for $U \leqslant 1.6$. A bond-order wave might separate the two insulating phases, as is found in the one-dimensional extended Hubbard model [16–18]. Therefore the line separating the Mott-Hubbard insulator and charge-density-wave insulator should be taken as a guide to the eye only.

In this paper we focus on the transitions between the metallic Luttinger liquid and the two insulating phases. We determine $V_c(U)$ for fixed $0 \leqslant v = V/U \leqslant 0.7$ with increment $\Delta v = 0.1$ and for fixed $U = 0.2$; for the meaning of the error bars in Fig. 1, see Sec. IV.

We note the following.

(i) In the absence of a nearest-neighbor interaction, the Mott-Hubbard transition is known to occur at $U_c(V = 0) = 1$ [2,20] which is well reproduced using the DMRG method [23]. The repulsive nearest-neighbor interaction *increases* the critical interaction strength; that is, the inclusion of the nearest-neighbor interaction stabilizes the *metallic* phase. Apparently, the additional repulsive nearest-neighbor interaction softens the two-particle scattering potential that is purely local in the bare Hubbard model. As a major result we find that the Mott transition remains continuous in the presence of a nearest-neighbor interaction. We presume that short-range interactions that decrease as a function of the particle distance will not fundamentally alter this behavior.

(ii) The transition from the Luttinger liquid metal to the charge-density-wave insulator is fairly common in the sense that even Hartree-Fock theory qualitatively reproduces the transition for not-too-large interactions. In Fig. 1, the corresponding Hartree-Fock prediction is shown as a dotted line. As usual, Hartree-Fock theory overestimates the stability of the ordered state and thus underestimates the critical interaction, $V^{\mathrm{HF}}_{c,\mathrm{CDW}}(U) < V_{c,\mathrm{CDW}}(U)$. Since the metallic phase extends well beyond the line $V = U/2$, there is no indication for a bond-order wave that might separate the Luttinger liquid and the charge-density-wave insulator.

We use a third-order spline interpolation through the data points to draw the phase transition lines in Fig. 1. The solid curves depict continuous quantum phase transitions in the sense that the gaps open and close continuously at the same critical interaction when the transition is approached from the metallic and insulating sides, respectively.

The endpoint of both solid curves where all three phases meet deserves special attention. Unsurprisingly, finite-size corrections are most severe in this region of phase space, and the study of the region around the tricritical point is cumbersome and beyond the scope of our presentation.

### C. Outline

Our work is organized as follows. In Sec. II we define the Hubbard model with long-range electron transfers and on-site and nearest-neighbor Coulomb interactions. We introduce the ground-state properties of interest, namely, the ground-state energy, the two-particle gap, the momentum distribution, and the density-density correlation function from which we determine the Luttinger parameter in the metallic phase and the CDW order parameter. In Sec. III we present results for the ground-state properties and discuss their finite-size dependencies and extrapolations to the thermodynamic limit where appropriate.

In Sec. IV we focus on the Mott-Hubbard transition in the presence of a nearest-neighbor interaction. We propose and discuss several methods to extract the critical interaction strength for the Mott transition based on the ground-state energy, the two-particle gap, the Luttinger parameter, and the structure factor whereby we study the Mott transition at fixed $v \equiv V/U$ in the range $0 \leqslant v \leqslant 0.7$ (increment $\Delta v = 0.1$) in units of the bandwidth, $W \equiv 1$. In addition, we address the Mott transition as a function of $V$ for fixed $U = 0.2$ and $U = 1.7$.

Short conclusions (Sec. V) close our presentation. The Hartree-Fock calculations for the CDW transition are collected in the Appendix.

## II. HUBBARD MODEL WITH LINEAR DISPERSION

### A. Hamiltonian

In this paper, we address the $1/r$-Hubbard model [2,20] with nearest-neighbor interactions

$$\hat{H} = \hat{T} + U\hat{D} + V\hat{V} \tag{1}$$

on a ring with $L$ sites (where $L$ is even). We discuss the kinetic energy and the Coulomb interaction terms separately.

#### 1. Kinetic energy

The kinetic energy describes the tunneling of electrons with spin $\sigma = \uparrow, \downarrow$ along a ring with $L$ sites,

$$\hat{T} = \sum_{\substack{l,m=1 \\ l\neq m;\sigma}}^{L} t(l-m)\hat{c}^{+}_{l,\sigma}\hat{c}_{m,\sigma}, \tag{2}$$

$$t(r) = (-\mathrm{i}t)\frac{(-1)^r}{d(r)},$$

$$d(r) = \frac{L}{\pi}\sin\left(\frac{\pi r}{L}\right). \tag{3}$$

The creation and annihilation operators $\hat{c}^{+}_{l,\sigma}$, $\hat{c}_{l,\sigma}$ for an electron with spin $\sigma = \uparrow, \downarrow$ on lattice site $l$ obey the usual anticommutation relations for fermions.

In Eq. (3), $d(l-m)$ is the chord distance between the sites $l$ and $m$ on a ring. In the thermodynamic limit and for $|l-m| \ll L$ fixed, we have $d(l-m) = (l-m) + O(1/L^2)$, and the decay of the electron transfer amplitude between the two sites is inversely proportional to their distance ("$1/r$-Hubbard model").

Since $L$ is even, we have antiperiodic electron transfer amplitudes because $d(L+r) = -d(r)$. Therefore we must choose antiperiodic boundary conditions

$$\hat{c}_{L+l,\sigma} = -\hat{c}_{l,\sigma} \tag{4}$$

for the operators, too. With these boundary conditions, the kinetic energy operator is diagonal in Fourier space,

$$\hat{C}^{+}_{k,\sigma} = \frac{1}{\sqrt{L}}\sum_{l=1}^{L} e^{\mathrm{i}kl}\hat{c}^{+}_{l,\sigma},$$

$$\hat{c}^{+}_{l,\sigma} = \frac{1}{\sqrt{L}}\sum_{k} e^{-\mathrm{i}kl}\hat{C}^{+}_{k,\sigma},$$

$$k = \frac{(2m+1)\pi}{L}, \quad m = -\frac{L}{2}, \ldots, \frac{L}{2} - 1, \tag{5}$$

so that

$$\hat{T} = \sum_{k,\sigma} \epsilon(k)\hat{C}^{+}_{k,\sigma}\hat{C}_{k,\sigma}, \quad \epsilon(k) = tk. \tag{6}$$

The dispersion relation of the $1/r$-Hubbard model is linear. We set

$$t = \frac{1}{2\pi} \tag{7}$$

so that the bandwidth is unity, $W \equiv 1$.

In this paper, we focus on the case of a paramagnetic half-filled ground state where we have the same number of electrons per spin species, $N_\uparrow = N_\downarrow$, that equals half the number of lattice sites, $N_\sigma = L/2$ ($\sigma = \uparrow, \downarrow$).

Equation (6) shows why Umklapp scattering is absent in the $1/r$-Hubbard model, so that the Mott transition occurs at finite interaction strengths. For noninteracting electrons at half band filling, all states from $k = -\pi$ are filled up to the single Fermi point at $k_\mathrm{F} = 0$. A scattering of particles from the opposite "Fermi" point, $k_- = -\pi$, requires high energies because a gap of $\Delta_\mathrm{B} = W$ has to be overcome for small momentum transfers, and a scattering energy of half of that gap is required for momentum transfers of half a reciprocal lattice vector, $q = \pi$. Therefore, in the field-theoretical limit [25], the $1/r$-Hubbard model reduces to a bare $g_4$ model because all other scattering processes, especially Umklapp scattering, are gapped. Corrections to the field-theory predictions are expected to be exponentially small for small interactions; see, e.g., Sec. IV C for the Luttinger parameter.

#### 2. Coulomb interaction

The Coulomb interaction is parametrized by two terms in Eq. (1). The on-site (Hubbard) interaction [4–6] acts locally between two electrons with opposite spins,

$$\hat{D} = \sum_{l=1}^{L} \hat{n}_{l,\uparrow}\hat{n}_{l,\downarrow}, \quad \hat{n}_{l,\sigma} = \hat{c}^{+}_{l,\sigma}\hat{c}_{l,\sigma}, \tag{8}$$

where $\hat{n}_{l,\sigma}$ counts the number of electrons with spin $\sigma$ on site $l$ and $\hat{n}_l = \hat{n}_{l,\uparrow} + \hat{n}_{l,\downarrow}$ counts the number of electrons on site $l$. The corresponding operators for the total number of electrons with spin $\sigma = \uparrow, \downarrow$ are denoted by $\hat{N}_\sigma = \sum_l \hat{n}_{l,\sigma}$, and $\hat{N} = \hat{N}_\uparrow + \hat{N}_\downarrow$.

To discuss the influence of the extended nature of the Coulomb interaction, we consider the case of pure

nearest-neighbor interactions,

$$\hat{V} = \sum_{l=1}^{L} (\hat{n}_l - 1)(\hat{n}_{l+1} - 1), \tag{9}$$

where we disregard the long-range parts of the Coulomb interaction for distances $|l - m| \geqslant 2$. The model in Eq. (1) describes the "extended" $1/r$-Hubbard model with on-site interaction $U$ and nearest-neighbor interaction $V$.

As we shall show in this paper, the Mott-Hubbard transition at half band filling remains continuous in the presence of short-range interactions. For not-too-large interactions and for $V \lesssim U/2$, the model contains a transition from the Luttinger liquid metal to the Mott-Hubbard insulator. For larger nearest-neighbor interactions, the model eventually describes transitions from the metallic state to a charge-density-wave (CDW) insulator. For strong interactions, $U \gg W$, the model contains a transition from the Mott-Hubbard insulator to the CDW insulator around $V \approx U/2$.

We study several values for the ratio $v = V/U$, namely, $v = 0, 0.1, 0.3, 0.4, 0.5, 0.6, 0.7$ for weak to strong nearest-neighbor interactions. Since we scan the value of $U$, we must limit the number of values for $v$ to keep the numerical effort within bounds when we include systems up to $L_{\max} = 80$ lattice sites; when finite-size effects are well behaved, e.g., for the ground-state energy, we limit our investigations to $L = 64$. Moreover, we scan $V$ for fixed $U = 0.2$ and $U = 1.7$ to study the Mott transition as a function of the nearest-neighbor interaction.

#### 3. Particle-hole symmetry

Under the particle-hole transformation

$$\hat{c}_{l,\sigma} \mapsto \hat{c}^{+}_{l,\sigma}, \quad \hat{n}_{l,\sigma} \mapsto 1 - \hat{n}_{l,\sigma}, \tag{10}$$

the kinetic energy remains unchanged,

$$\begin{aligned} \hat{T} &\mapsto \sum_{\substack{l,m=1 \\ l\neq m;\sigma}}^{L} t(l-m)\hat{c}_{l,\sigma}\hat{c}^{+}_{m,\sigma} \\ &= \sum_{\substack{l,m=1 \\ l\neq m;\sigma}}^{L} [-t(m-l)]\hat{c}^{+}_{l,\sigma}\hat{c}_{m,\sigma} = \hat{T}, \end{aligned} \tag{11}$$

because $t(-r) = -t(r)$. Furthermore,

$$\hat{D} \mapsto \sum_{l=1}^{L} (1 - \hat{n}_{l,\uparrow})(1 - \hat{n}_{l,\downarrow}) = \hat{D} - \hat{N} + L, \tag{12}$$

and

$$\hat{V} \mapsto \hat{V}. \tag{13}$$

Therefore $\hat{H}(N_\uparrow, N_\downarrow)$ has the same spectrum as $\hat{H}(L - N_\uparrow, L - N_\downarrow) - U(2L - N) + LU$, where $N = N_\uparrow + N_\downarrow$ is the particle number.

### B. Ground-state properties

We are interested in the metal-insulator transition at half band filling where the metallic Luttinger liquid for weak interactions turns into a paramagnetic Mott insulator for large interactions at some finite value $U_c(V)$ when $V$ is small enough or it turns into a CDW insulator for strong nearest-neighbor interactions. The metal-insulator transition can be inferred from the finite-size extrapolation of the ground-state energy and of the two-particle gap [23]. Alternatively, the Luttinger parameter [26] and the finite-size extrapolation of the structure factor at the Brillouin zone boundary permit us to determine the critical interaction strength. Moreover, the charge-density-wave state can be monitored by the CDW order parameter. In this section, we also introduce the momentum distribution for finite systems that is also accessible via the DMRG method.

#### 1. Ground-state energy and two-particle gap

We denote the ground-state energy by

$$E_0(N, L; U, V) = \langle \Psi_0 | \hat{H} | \Psi_0 \rangle \tag{14}$$

for given particle number $N$, system size $L$, and interaction parameters $U, V$. Here, $|\Psi_0\rangle$ is the normalized ground state of the Hamiltonian (1). We are interested in the thermodynamic limit, $N, L \to \infty$ with $n = N/L$ fixed. We denote the ground-state energy per site and its extrapolated value by

$$\begin{aligned} e_0(N, L; U, V) &= \frac{1}{L} E_0(N, L; U, V), \\ e_0(n; U, V) &= \lim_{L\to\infty} e_0(N, L; U, V), \end{aligned} \tag{15}$$

respectively.

The two-particle gap is defined by

$$\Delta_2(L; U, V) = \mu_2^{+}(L; U, V) - \mu_2^{-}(L; U, V), \tag{16}$$

where

$$\begin{aligned} \mu_2^{-}(L; U, V) &= E_0(L, L; U, V) - E_0(L-2, L; U, V), \\ \mu_2^{+}(L; U, V) &= E_0(L+2, L; U, V) - E_0(L, L; U, V) \end{aligned} \tag{17}$$

are the chemical potentials for adding the last two particles to half filling and the first two particles beyond half filling, respectively.

Due to particle-hole symmetry, we have

$$\mu_2^{-}(L; U, V) = 2U - \mu_2^{+}(L; U, V), \tag{18}$$

so that

$$\Delta_2(L; U, V) = 2\mu_2^{+}(L; U, V) - 2U \tag{19}$$

and

$$\Delta_2(U, V) = \lim_{L\to\infty} \Delta_2(L; U, V) \tag{20}$$

in the thermodynamic limit. We always consider the spin symmetry sector $S = S^z = 0$. For this reason, we study the two-particle gap rather than the single-particle gap.

The two added particles repel each other, so that, in the thermodynamic limit, they are infinitely separated from each other. Therefore we have

$$\Delta_2(U, V) = 2\Delta_1(U, V), \tag{21}$$

where $\Delta_1(U, V)$ is the gap for single-particle excitations. For finite systems, we expect the interaction energy

$$e_R(L; U, V) = \Delta_2(L; U, V) - 2\Delta_1(L; U, V) = O(1/L) > 0 \tag{22}$$

to be positive, of the order $1/L$. We verified that the interaction energy vanishes in the thermodynamic limit for the case $V = 0$ [23].

#### 2. Momentum distribution

We also study the spin-summed momentum distribution in the ground state at half band filling, $N = L$,

$$n_k(L;U,V) = \langle\Psi_0|\hat{n}_{k,\uparrow} + \hat{n}_{k,\downarrow}|\Psi_0\rangle = \sum_{l,m;\sigma} e^{ik(l-m)} P_{l,m;\sigma} \tag{23}$$

with $\hat{n}_{k,\sigma} = \hat{C}^+_{k,\sigma}\hat{C}_{k,\sigma}$ and the single-particle density matrix $P_{l,m;\sigma} = \langle\Psi_0|\hat{c}^+_{l,\sigma}\hat{c}_{m,\sigma}|\Psi_0\rangle$. Due to particle-hole symmetry we have

$$n_k(L;U,V) = 1 - n_{-k}(L;U,V) \tag{24}$$

at half band filling. Therefore it is sufficient to study wave numbers from the interval $-\pi < k < 0$.

In our previous work, we showed that a bound state forms at the lower band edge in the bare $1/r$-Hubbard model right at the Mott transition. The nature of this bound state is not well understood and certainly deserves further studies. Its presence gives rise to a Fano resonance in the spectral function that is discernible in the slope of the momentum distribution at the band edge. Unfortunately, this specific feature cannot be used to trace the Mott-Hubbard transition in the extended $1/r$-Hubbard model because the bound state apparently moves away from the band edge for $V > 0$, erasing the Fano resonance shape in the slope of the momentum distribution at the band edge.

#### 3. Density-density correlation function and Luttinger parameter

Lastly, we address the density-density correlation function at half band filling, $N = L$,

$$C^{\mathrm{NN}}(r,L;U,V) = \frac{1}{L}\sum_{l=1}^{L}(\langle\hat{n}_{l+r}\hat{n}_l\rangle - \langle\hat{n}_{l+r}\rangle\langle\hat{n}_l\rangle), \tag{25}$$

where $\langle\cdots\rangle \equiv \langle\Psi_0|\cdots|\Psi_0\rangle$. The limit $L \gg r \gg 1$ for $U, V \ll W$ is also accessible from field theory [25,27,28],

$$C^{\mathrm{NN}}(r \gg 1;U,V) \sim -\frac{K(U,V)}{(\pi r)^2} + \frac{A(U,V)(-1)^r}{r^{1+K}[\ln(r)]^{3/2}} + \cdots, \tag{26}$$

where $A(U,V)$ is a constant that depends on the interaction but not on the distance $r$.

We extract the Luttinger exponent $K(U,V)$ from the structure factor,

$$\tilde{C}^{\mathrm{NN}}(q,L;U,V) = \sum_{r=0}^{L-1} e^{-iqr} C^{\mathrm{NN}}(r,L;U,V), \tag{27}$$

where the wave numbers are from momentum space, $q = (2\pi/L)m_q$, $m_q = -L/2, -L/2+1, \ldots, L/2-1$. By construction, $\tilde{C}^{\mathrm{NN}}(q=0,L;U,V) = 0$ because the particle number is fixed, $N = L$ in the half-filled ground state. In the thermodynamic limit, the structure factor $\tilde{C}^{\mathrm{NN}}(q,L;U,V)$ remains of the order unity even in the CDW phase because we subtract the contributions of the long-range order in the definition (25).

The transition to a charge-density-wave insulator can be monitored from the CDW order parameter. In this paper, we do not study the standard CDW order parameter,

$$D(L;U,V) = \frac{1}{L}\left|\sum_{r=0}^{L-1}(-1)^r(\langle\hat{n}_r\rangle - 1)\right| \leqslant 1. \tag{28}$$

Instead, we include all short-range contributions and address

$$N_\pi(L;U,V) = \frac{1}{L}\sum_{r=0}^{L-1}(-1)^r\frac{1}{L}\sum_{l=0}^{L-1}(\langle\hat{n}_{r+l}\hat{n}_l\rangle - 1). \tag{29}$$

When the charges are distributed homogeneously, $\langle\hat{n}_l\rangle = 1$, we have $N_\pi(L;U,V) = \tilde{C}^{\mathrm{NN}}(\pi,L;U,V)/L$, and the order parameter vanishes in the metallic phase. More generally, in the thermodynamic limit we have $N_\pi(U,V) = (D(U,V))^2$. In the $1/r$-Hubbard model with its long-range electron transfer, it is advantageous to analyze $N_\pi(L;U,V)$ to facilitate a reliable finite-size analysis.

When Eq. (26) is employed, it follows that the Luttinger parameter for finite systems,

$$K(L;U,V) = \frac{L}{2}\tilde{C}^{\mathrm{NN}}(2\pi/L,L;U,V), \tag{30}$$

can be used to calculate the Luttinger parameter in the thermodynamic limit,

$$K(U,V) = \lim_{L\to\infty} K(L;U,V) = \pi\lim_{q\to 0}\frac{\tilde{C}^{\mathrm{NN}}(q;U,V)}{q}, \tag{31}$$

where we denote the structure factor in the thermodynamic limit by $\tilde{C}^{\mathrm{NN}}(q;U,V)$. Using Eq. (31), the Luttinger exponent can be calculated numerically with very good accuracy [29]. The Luttinger parameter can be used to locate the metal-insulator transition in one spatial dimension.

## III. GROUND-STATE PROPERTIES

Before we investigate the Mott transition for the half-filled extended $1/r$-Hubbard model in more detail in the next section, we present DMRG results for the ground-state energy, the two-particle gap, the momentum distribution, the structure factor, and the CDW order parameter. For the numerical calculations we employ a DMRG code that permits the treatment of an arbitrary quantum system with long-ranged complex interactions. It uses non-Abelian symmetries and optimization protocols inherited from quantum information theory [30]. The accuracy is controlled via the dynamic block-state selection (DBSS) approach [31,32], where the *a priori* value for the truncation errors was set to $10^{-6}$. Further technical details of the DMRG implementation can be found in Ref. [23]. Note that our finite-size scaling analysis requires very accurate data. We obtain those by imposing strict accuracy settings in our DMRG code and by restricting the largest system size to $L_{\max} = 80$ to limit the truncation errors.

### A. Ground-state energy

For $V = 0$, the ground-state energy per site for finite system sizes is given by ($n = N/L$, where $N$ is even) [2,20,23]

$$e_0 = \frac{1}{4}n(n-1) + \frac{U}{4}n - \frac{1}{2L}\sum_{r=0}^{(N/2)-1}\sqrt{1+U^2-4U(2r+1-L/2)/L} \tag{32}$$

with the abbreviation $e_0 \equiv e_0(N, L; U, V = 0)$.

In the thermodynamic limit and at half band filling, $n = 1$, the ground-state energy per site becomes particularly simple,

$$e_0(n=1; U \leqslant 1, V=0) = -\frac{1}{4} + \frac{U}{4} - \frac{U^2}{12},$$
$$e_0(n=1; U \geqslant 1, V=0) = -\frac{1}{12U}. \tag{33}$$

The analytic expressions (32) and (33) are useful for a comparison with numerical data at $V = 0$.

For finite $V$, we can use first-order perturbation theory for weak interactions, $U, V \ll 1$, to find

$$e_0^{\mathrm{PT}}(U,V) = -\frac{1}{4} + \frac{U}{4}\left(1 - \frac{8v}{\pi^2}\right) + O(U^2) \tag{34}$$

with $v = V/U$ in the thermodynamic limit and at half band filling. Note that Eq. (34) holds for all $v$, as long as $U, V \ll 1$.

We display the ground-state energy per site at half band filling, $e_0(L, L; U, V)$, as a function of the inverse system size ($L = 8, 16, 24, 32, 48, 64$) and various values of $U$ in Figs. 2(a) ($v = 0.1$), 2(b) ($v = 0.3$), and 2(c) ($v = 0.5$). For the extrapolation to the thermodynamic limit, we use the algebraic fit function

$$e_0(L, L; U, V) = e_0(n=1; U, V) + a_0(U, V)\left(\frac{1}{L}\right)^{\gamma_0(U,V)}, \tag{35}$$

where $e_0(n = 1; U, V)$ denotes the numerical estimate for the ground-state energy density in the thermodynamic limit and $a_0(U, V)$ and $\gamma_0(U, V)$ are the two other fit parameters. This extrapolation scheme is appropriate for $V = 0$ [23] because the ground-state energy per site scales with $(1/L)^2$ for $U \neq 1$ and with $(1/L)^{3/2}$ for $U = U_c(V = 0) = 1$, as follows from Eq. (32). More generally, we *assume* for all $(U, V)$

$$\gamma_0(U,V) = \begin{cases} 2 & \text{for } U \neq U_c(V) \\ \frac{3}{2} & \text{for } U = U_c(V). \end{cases} \tag{36}$$

Here, we follow the common notion that the ground-state energy density displays generic $(1/L)^2$ finite-size corrections if the model is not critical. When the holon dispersion displays a square-root divergence at low energies for $U_c(V)$, the exponent is reduced to $\gamma_0(U_c(V), V) = 3/2$, as in the case of the bare $1/r$-Hubbard model. These exponents apply for very large system sizes. We shall discuss the finite-size modifications in detail in Sec. IV.

The extrapolated ground-state energies are shown in Fig. 3 together with the exact result for $V = 0$. For small

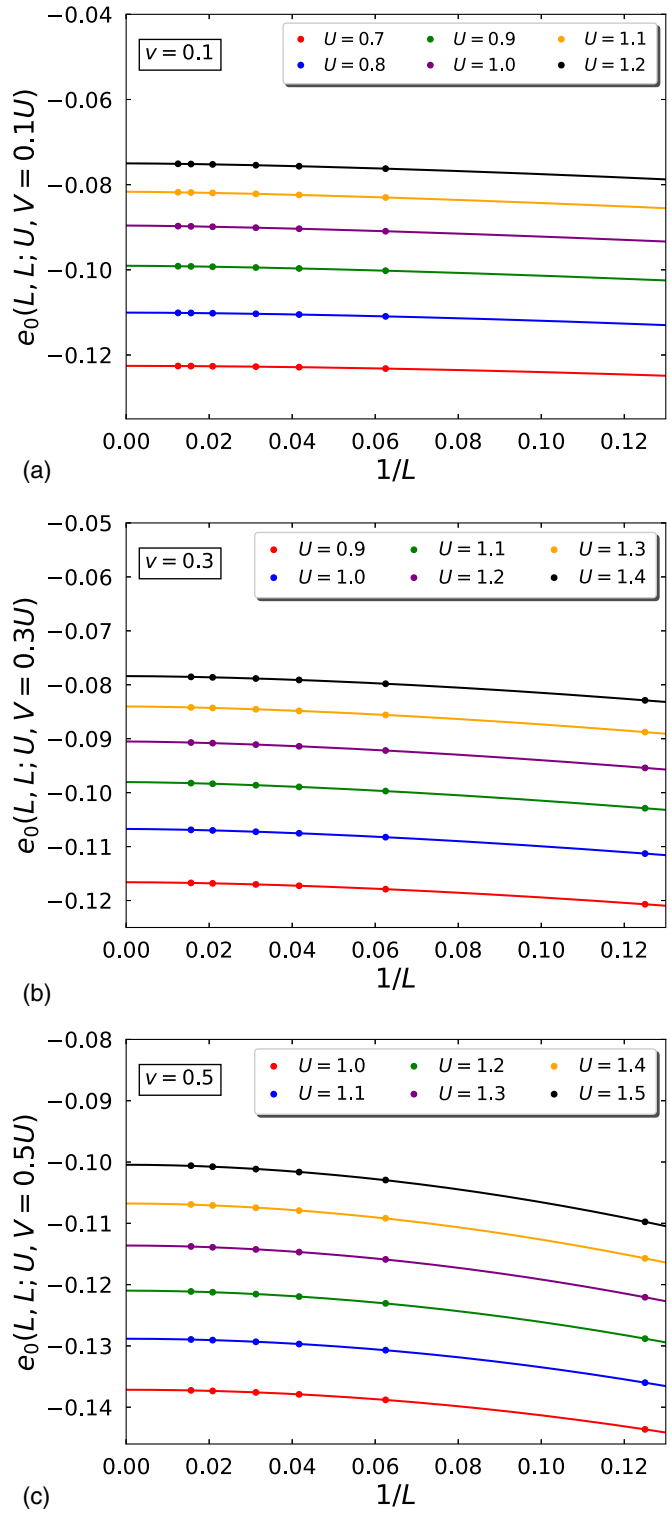


FIG. 2. Ground-state energy per lattice site at half band filling, $e_0(L, L; U, V)$, for the extended $1/r$-Hubbard model as a function of $1/L$ for $L = 8, 16, 24, 32, 48, 64$ and various values for $U$ for (a) $v = 0.1$, (b) $v = 0.3$, and (c) $v = 0.5$. The solid curves are fits to the algebraic fit function (35). The intercept of the extrapolation curves with the ordinate defines the extrapolation estimate $e_0(n = 1; U, V)$ in the thermodynamic limit.

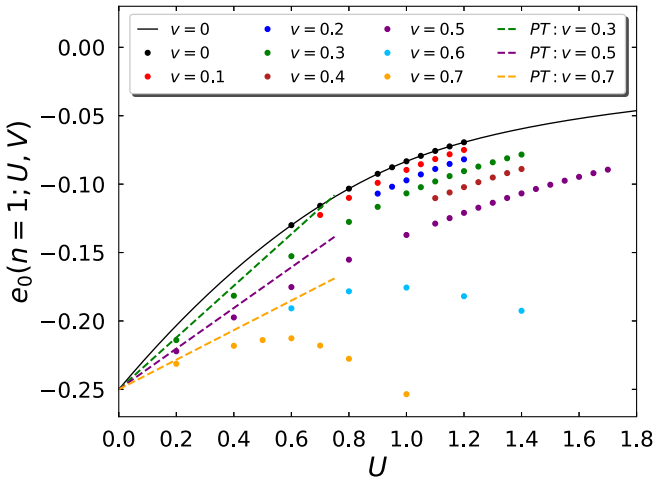


FIG. 3. Ground-state energy per lattice site at half band filling in the thermodynamic limit, $e_0(n = 1; U, V)$, for the extended $1/r$-Hubbard model from the extrapolation to the thermodynamic limit in Fig. 2. The dashed lines represent first-order order perturbation theory (PT) for $v = V/U = 0.3, 0.5, 0.7$; see Eq. (34). The solid curve is the exact result for $V = 0$, $e_0(n = 1; U, V = 0)$; see Eq. (33).

interactions, the nearest-neighbor interaction in the particle-hole-symmetric form decreases the ground-state energy because the Hartree contribution at half band filling is subtracted in the definition of the interaction, and the Fock contribution is negative because of the exchange hole. Therefore the linear term in the interaction $(U/4)(1 - 8v/\pi^2)$ [see Eq. (34)] is smaller in the presence of a nearest-neighbor interaction.

At large interactions, the ground-state energy approaches zero, $\lim_{U\to\infty} e_0(n = 1; U, V = vU) = 0$, as long as the charge density wave is absent. In the presence of a CDW, the ground-state energy is negative and proportional to $U$, $e_0(U \gg 1, V) = U(1/2 - v)$. Therefore the ground-state energy displays a maximum for $v = 0.6$ and $v = 0.7$ because its slope as a function of $U$ is positive for small interactions and negative for large interaction strengths in the CDW phase.

### B. Two-particle gap

For $V = 0$ the two-particle gap is known exactly for all system sizes [2,20,23],

$$\Delta_2(L; U \geqslant 1, V = 0) = U - 1 + \frac{2}{L} + \sqrt{(U-1)^2 + \frac{4U}{L}}. \tag{37}$$

In the thermodynamic limit, we find

$$\Delta_2(U \geqslant 1, V = 0) = 2(U - 1). \tag{38}$$

The gap opens linearly above the critical interaction strength, $U_c(U, V = 0) = 1$. Equation (37) shows that the finite-size data approach the value in the thermodynamic limit

$$\Delta_2(L; U, V) = \Delta_2(U, V) + a_2(U, V)\left(\frac{1}{L}\right)^{\gamma_2(U,V)} \tag{39}$$

with $\gamma_2(U \neq U_c, V = 0) = 1$, $\gamma_2(U = U_c, V = 0) = 1/2$.

More generally, we *assume* for all $(U, V)$

$$\gamma_2(U, V) = \begin{cases} 1 & \text{for } U \neq U_c(V) \\ \frac{1}{2} & \text{for } U = U_c(V). \end{cases} \tag{40}$$

As for the ground-state energy, these exponents apply for very large system sizes. We shall discuss the finite-size modifications in more detail in Sec. IV.

In Fig. 4 we show the DMRG results for $\Delta_2(L; U, V)$ as a function of $1/L$ for $L = 8, 16, 24, 32, 48, 64$ and various values of $U$ for $v = 0.1$ [Fig. 4(a)], $v = 0.3$ [Fig. 4(b)], and $v = 0.5$ [Fig. 4(c)]. The curves are fits to the algebraic function in Eq. (39). The fits in Fig. 4 are seen to agree very well with the data, showing a steep decrease of the finite-size gap as a function of inverse system size. This indicates that large system sizes are required to obtain reasonable gap extrapolations.

The extrapolated gaps $\Delta(U, V)$ are shown in Fig. 5 as a function of $U$ for $v = 0$, $v = 0.1$, $v = 0.3$, and $v = 0.5$. Apparently, the nearest-neighbor interaction not only shifts the critical interaction to higher values, but also reduces the size of the gap in the Mott insulating phase. The extrapolated gaps becomes *smaller* as a function of $V$; that is, the nearest-neighbor interaction *reduces* the tendency to form a Mott-Hubbard insulator. Note that gaps from finite-size extrapolations are least accurate close to the transition, so that they tend to "smear out" sharp transitions. For an elaborate discussion, see Ref. [23].

At first sight, the *increase* of the critical interaction is counterintuitive because one might argue that an additional repulsive nearest-neighbor Coulomb interaction should favor the insulating state, not the metallic state. From a wave-mechanical viewpoint, however, the repulsive nearest-neighbor interaction softens the two-particle scattering potential. Figuratively speaking, particles that are scattered by the weaker nearest-neighbor interaction $V$ do not experience the stronger on-site interaction $U$. For a quantitative analysis, see Sec. IV.

When $v = V/U$ is small, the change in the critical interaction strength is also small, and one might think of using perturbation theory around the bare $1/r$-Hubbard model. To test this idea, we consider

$$C(L; U, V) = \frac{e_0(L, L; U, V) - e_0(L, L; U, V = 0)}{V}. \tag{41}$$

In the limit $V \to 0$, leading-order perturbation theory gives

$$\lim_{V\to 0} C(L; U, V) = C^{\mathrm{NN}}(r = 1, L; U, V = 0), \tag{42}$$

where $C^{\mathrm{NN}}(r = 1, L; U, V = 0)$ is the nearest-neighbor density-density correlation function at half band filling for the bare $1/r$-Hubbard model at finite system sizes $L$; see Eq. (25). As an example, for $v = 0.3$ and $U \lesssim 0.7$, we find that $C^{\mathrm{NN}}(r = 1, L; U, V = 0)$ agrees fairly well with $C(L; U, V)$ from Eq. (41). Around the Mott transition, however, the corrections become sizable, more noticeably for larger systems. Therefore low-order perturbation theory around the limit $V = 0$ cannot be used to determine the critical interaction strength $U_c(V)$ reliably.

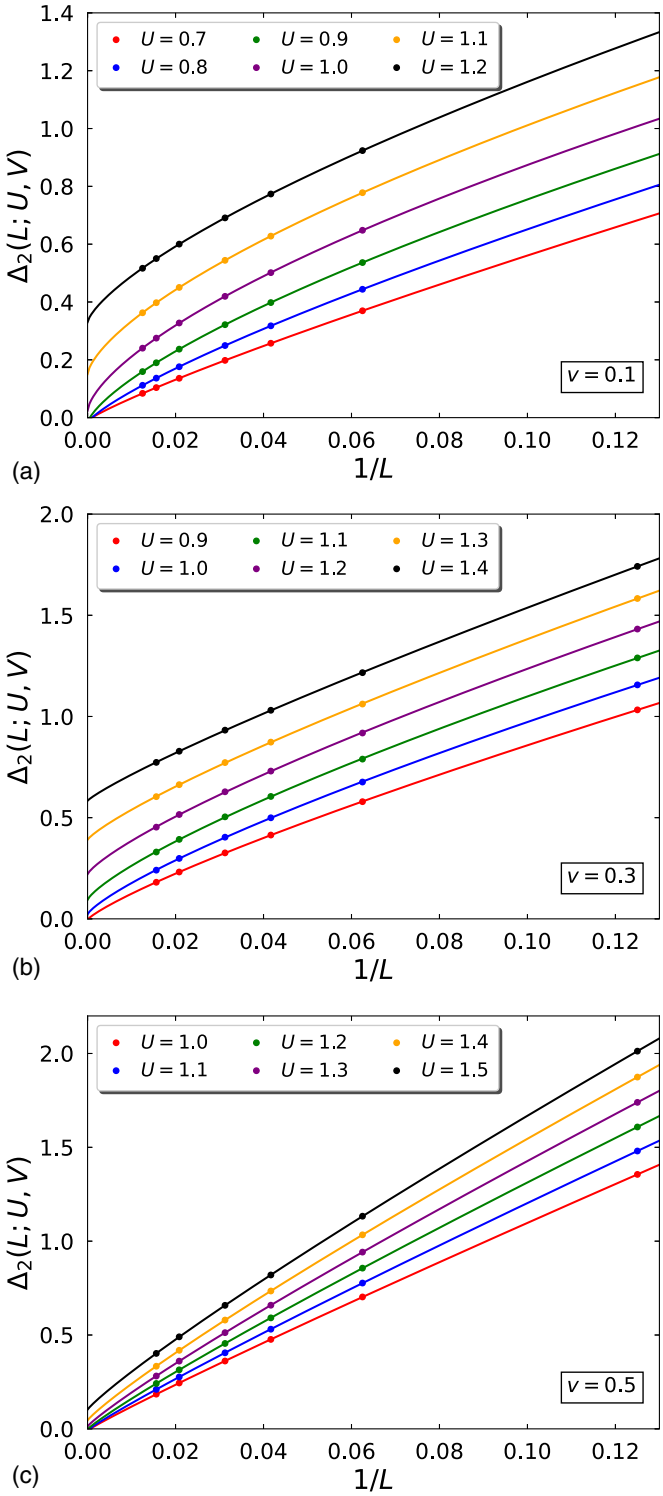


FIG. 4. Two-particle gap $\Delta_2(L;U,V)$ for the extended $1/r$-Hubbard model as a function of inverse system size for $L = 8, 16, 24, 32, 48, 64$ and various values of $U$ for (a) $v = 0.1$, (b) $v = 0.3$, and (c) $v = 0.5$. The solid curves are fits to the algebraic fit function (39). The intercept of the extrapolation curves with the ordinate defines the extrapolation estimate $\Delta_2(U,V)$ for the two-particle gap.

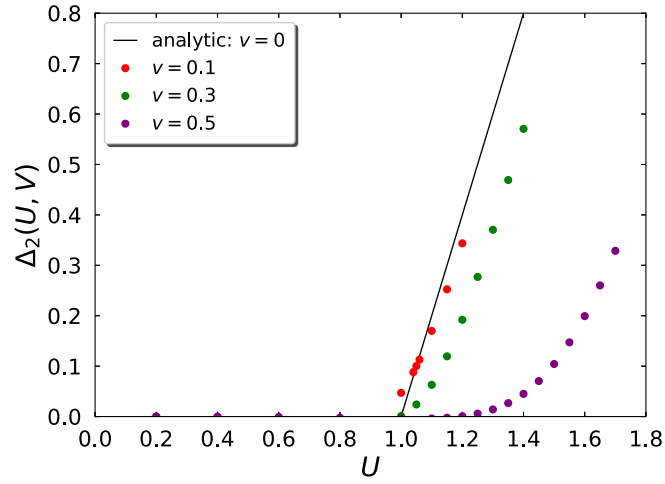


FIG. 5. Two-particle gap $\Delta_2(U,V)$ for the extended $1/r$-Hubbard model as a function of $U$ for $v = 0.1$ (red solid circles), $v = 0.3$ (green solid circles), and $v = 0.5$ (purple solid circles), extrapolated from finite-size data with up to $L = 64$ sites. The solid line is the exact result in the thermodynamic limit for $V = 0$, $\Delta_2(U, V = 0) = 2(U - 1)$; see Eq. (38).

### C. Momentum distribution

In Fig. 6 we show the momentum distribution from DMRG calculations at half band filling for $L = 64$ sites and various values of $U$ for $v = 0.1$, $v = 0.3$, and $v = 0.5$ [Figs. 6(a), 6(b), and 6(c), respectively]. For small interactions, the momentum distribution resembles that of a Fermi liquid with all states $-\pi < k < 0$ occupied and all states $0 < k < \pi$ empty. For small $U$, low-energy scattering processes are limited to the vicinity of the sole Fermi point $k_F = 0$. Indeed, in the field-theoretical limit, $U, V \ll 1$, the model reduces to a bare $g_4$ model of only right-moving particles [25]. This "noninteracting Luttinger liquid" displays a jump discontinuity at $k_F$.

However, the $1/r$-Hubbard model is defined on a lattice, and the bandwidth is finite. Consequently, the second Fermi point at $k_{F,2} = -\pi$ starts to play a role when $U$ becomes large, of the order of half the bandwidth. States near $k_{F,2}$ are depleted more quickly as a function of $U$ than those deeper in the Brillouin zone. Therefore, as seen in Fig. 6, the momentum distribution develops a maximum around $k = -\pi/2$, with a corresponding minimum around $k = \pi/2$.

These considerations show that the Luttinger parameter must deviate from unity, $K(U,V) < 1$, for all $(U,V)$, even though corrections to unity are (exponentially) small for $U, V \ll 1$. Therefore the momentum distribution is a continuous function in the (extended) $1/r$-Hubbard model for all $U, V > 0$.

In contrast to the case $V = 0$ [23], there is no Fano resonance discernible in the slope of the momentum distribution at $k = -\pi$ as the slope is always positive at $k = -\pi$. This indicates that the bound state for $V = 0$ moves away from the band edge for finite $V > 0$ and thus cannot be detected in the momentum distribution. Consequently, we cannot use the resonance to locate the metal-insulator transition in the extended $1/r$-Hubbard model.

### D. Structure factor and CDW order parameter

Lastly, we show the structure factor from DMRG calculations in Fig. 7 for $v = 0.1$, $v = 0.3$, and $v = 0.5$ [Figs. 7(a),

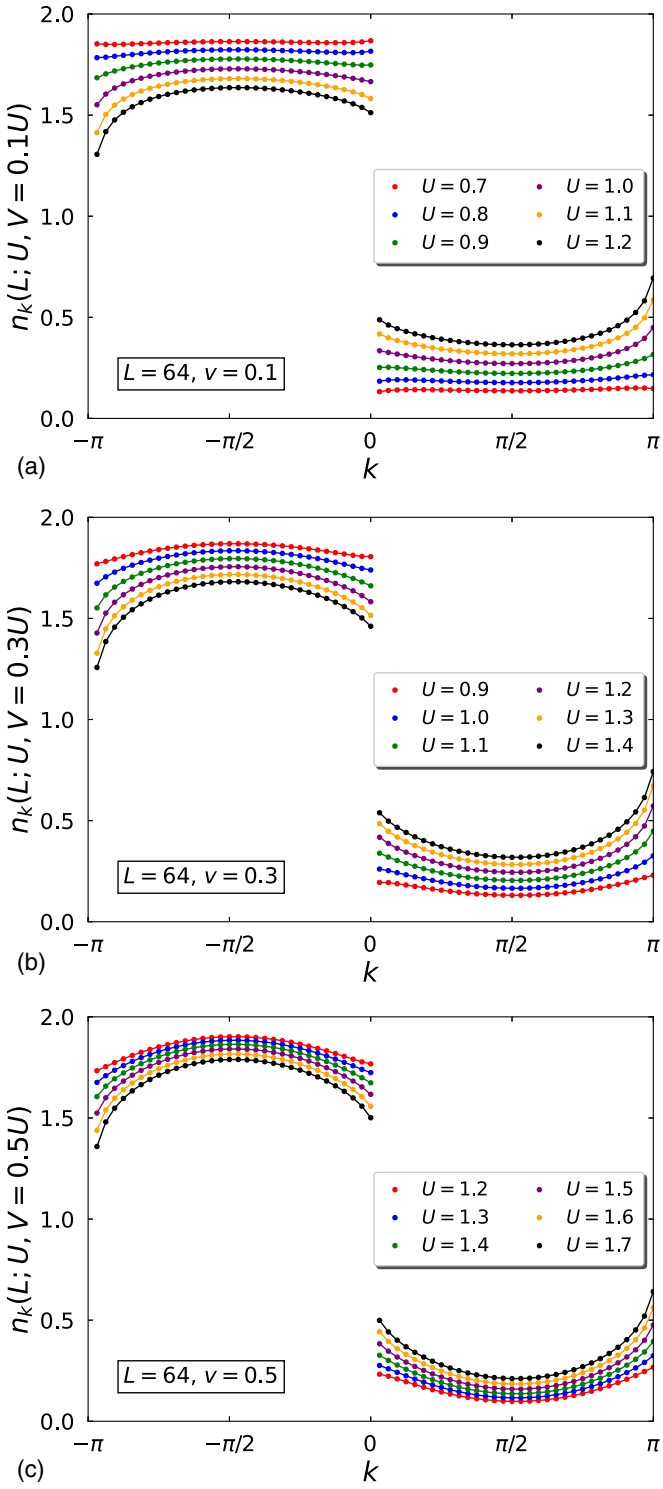


FIG. 6. Momentum distribution $n_k(L;U,V)$ from DMRG calculations at half band filling for the extended $1/r$-Hubbard model for $L=64$ sites and various values of $U$ for (a) $v=0.1$, (b) $v=0.3$, and (c) $v=0.5$.

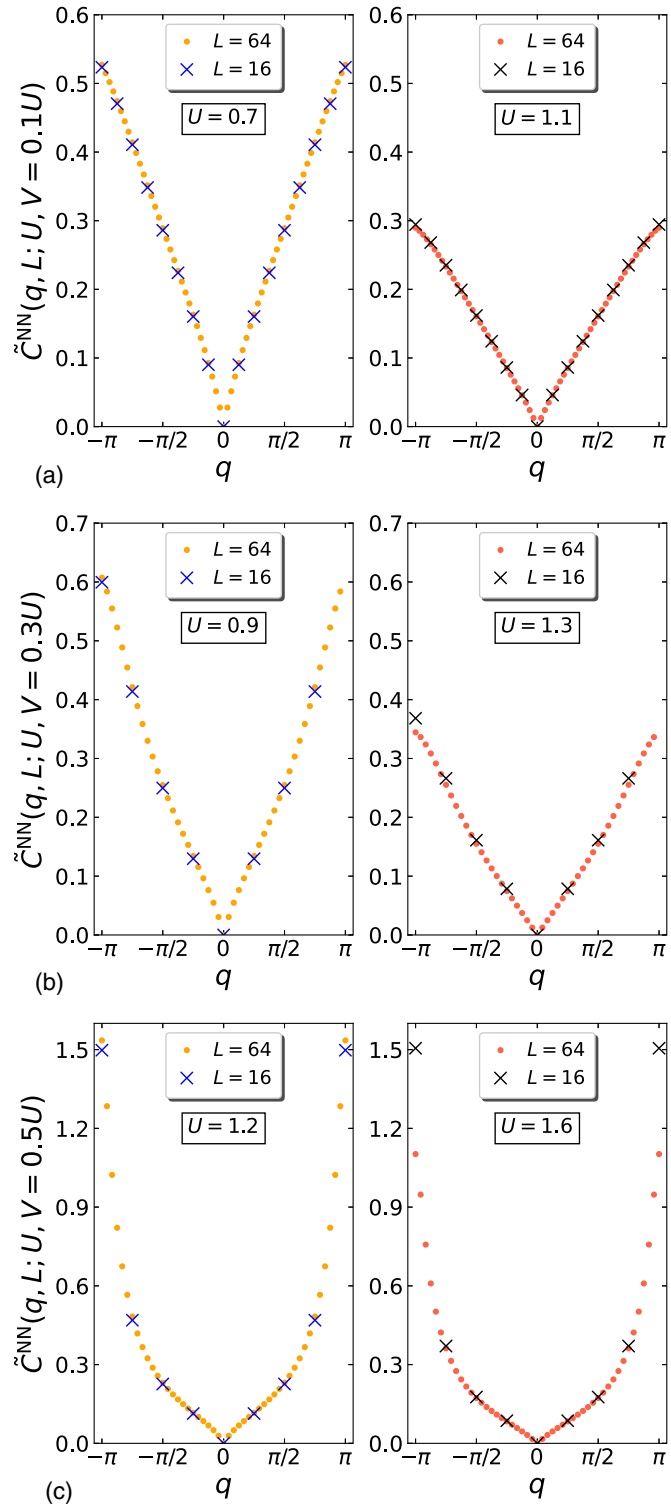


FIG. 7. Structure factor $\tilde{C}^{\mathrm{NN}}(q,L;U,V)$ for the extended $1/r$-Hubbard model for $L=16,64$ below (left panels) and above (right panels) the Mott transition for (a) $v=0.1$, (b) $v=0.3$, and (c) $v=0.5$.

7(b), and 7(c), respectively] for the extended $1/r$-Hubbard model at system sizes $L=16,64$ below (left panels) and above (right panels) the Mott transition. It is seen that the finite-size effects are fairly small but larger systems permit a much better resolution in momentum space. In comparison with the exact result for the noninteracting system,

$$\tilde{C}^{\mathrm{NN}}(q,n=1;U=0,V=0)=\frac{|q|}{\pi}, \tag{43}$$

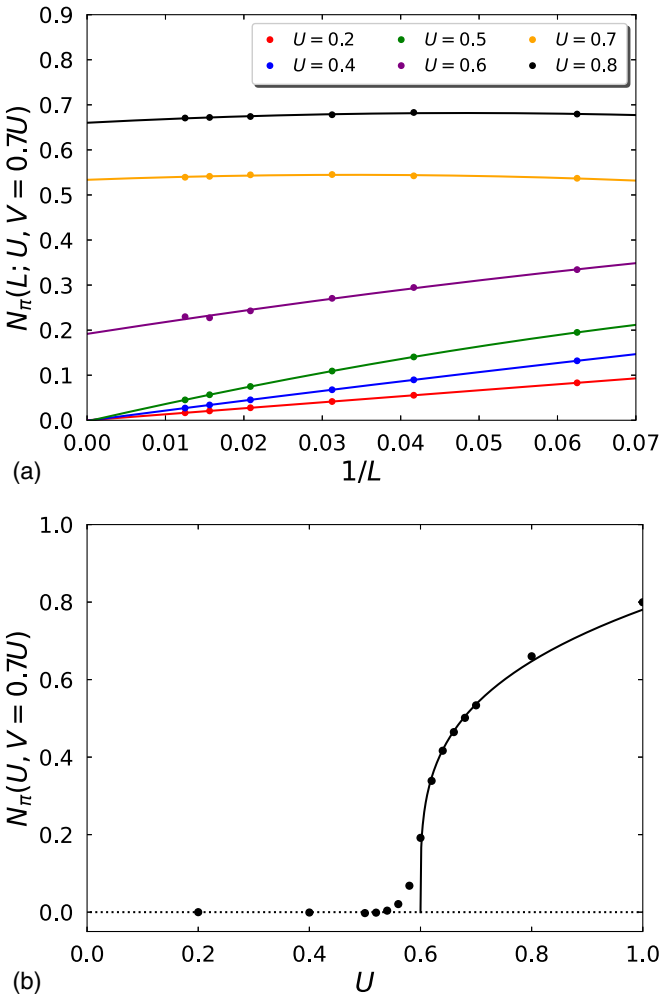


FIG. 8. (a) CDW order parameter $N_\pi(L;U,V)$ for the extended half-filled $1/r$-Hubbard model as a function of $1/L$ ($L \leqslant 80$) for $v = 0.7$ and various $U$ values. Curves are a second-order polynomial fit in $1/L$; see Eq. (44). (b) Extrapolated CDW order parameter $N_\pi(U, V = 0.7U)$ as a function of $U$. The curve is an algebraic fit to the data in the vicinity of the CDW transition [see Eq. (45)] with $U_c(v = 0.7) = 0.6$, $N_0 = 1$, and $2\nu = 0.3$.

we see that the local interaction reduces the charge fluctuations. This is expected because the suppression of double occupancies likewise reduces the number of holes and the charges are more homogeneously distributed in the system. Therefore the charge correlations become smaller when we compare the left and right panels in the same row.

The nearest-neighbor interaction counters the effect of the Hubbard interaction because nearest-neighbor pairs of a double occupancy and a hole are energetically favorable. Therefore the charge correlations increase when we go from Fig. 7(a) to Fig. 7(c) in the left or right row, even though $U$ also increases from Fig. 7(a) to Fig. 7(c).

When the nearest-neighbor interaction increases beyond a certain threshold value $V_c(U)$, the ground state displays charge-density-wave order. In Fig. 8(a) we show the charge-density-wave order parameter $N_\pi(L;U,V = 0.7U)$ [see Eq. (29)] as a function of $1/L$ for various values of $U$, and the extrapolated result $N_\pi(U, V = 0.7U)$ into the thermodynamic limit using a second-order polynomial fit in Fig. 8(b),

$$N_\pi(L;U,V) = N_\pi(U,V) + \frac{N_1(U,V)}{L} + \frac{N_2(U,V)}{L^2}. \quad (44)$$

Apparently, the CDW order parameter is continuous over the CDW transition. Close to the transition, $U \gtrsim U_c(V)$,

$$N_\pi(U,V) = N_0[U - U_c(V)]^{2\nu}, \quad (45)$$

where $\nu$ is the critical exponent for the CDW order parameter $D(U,V)$. Note that we pass the CDW transition for a fixed ratio $v = U/V$.

To make use of Eq. (45), the critical interaction $U_c(V)$ must be known. In addition, the region of validity of Eq. (45) is unknown *a priori*. Typically, one has to study system parameters close to the transition to obtain a reliable estimate for $\nu$. Therefore very large system sizes might be necessary to reach the scaling limit, and we have to be satisfied with the result from Fig. 8(b) that the CDW transition at $v = 0.7$ is continuous with exponent $\nu \leqslant 1/2$.

## IV. MOTT TRANSITION

In this section we determine the critical value for the Mott transition in the extended $1/r$-Hubbard model. We investigate the two-particle gap, the ground-state energy, the Luttinger parameter, and the structure factor at the Brillouin zone boundary to locate the critical interaction strength $U_c(V)$. The Mott transition remains continuous for all $V/U$.

### A. Two-particle gap

In our previous work [23], we showed that the exponent $\gamma_2(U) = \gamma_2(U, V = 0)$ sensitively depends on $U$ in the vicinity of the Mott-Hubbard transition, and the critical interaction for the $1/r$-Hubbard model, $U_c(V = 0) = 1$, was obtained with an accuracy of 1‰.

To illustrate this result for the bare $1/r$-Hubbard model, in Fig. 9 we show the extrapolated gap exponent $\gamma_2(U) \equiv \gamma_2(U, V = 0)$ using the analytic expression (37) for various combinations of system sizes in the range $L = 8, 16, 24, 32, 48, 64, 80, 96, 128, 256, 512, 1024, 2048, 4096$.

The extrapolation of finite-size data does not permit us to reproduce the jump discontinuity in Eq. (37). Instead, we observe a continuous curve as a function of the interaction with a minimum close to criticality. The minimal value for $\gamma_2(U)$ depends on the selected range of system sizes. The gap exponent in the thermodynamic limit [see Eq. (40)] cannot be reproduced from finite-size studies, but it is approached systematically with increasing system size. Furthermore, it can be seen from Fig. 9 that the inclusion of smaller system sizes such as $L = 8, 16$ leads to stronger deviations so that the smallest system sizes should be discarded. Note, however, that the *position* of the minimum and thus the critical interaction strength are very well reproduced in all cases. Therefore the minimum of $\gamma_2(U, V)$ permits us to locate the Mott transition $U_c(V)$ fairly accurately.

In Fig. 10 we display the exponent $\gamma_2(U, V)$, as obtained from the fit of the finite-size data in the range $16 \leqslant L \leqslant 80$ to the algebraic function in Eq. (39). Also shown in the figure are

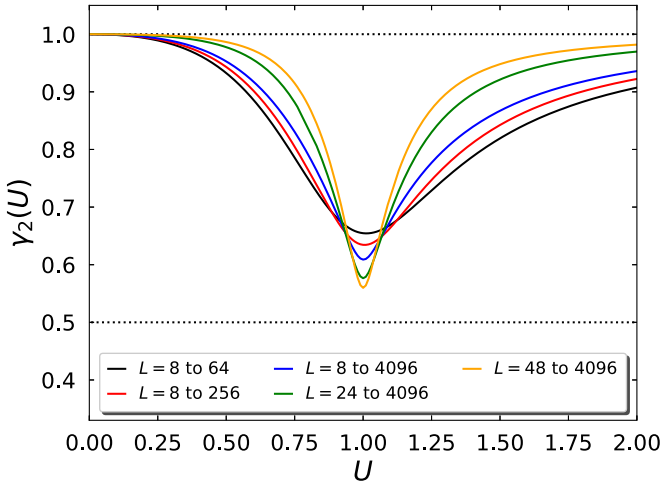


FIG. 9. Extrapolated gap exponent $\gamma_2(U) = \gamma_2(U, V = 0)$ using the analytical expression of the two-particle gap in Eq. (37). Various system sizes are used, in the range $L = 8, 16, 24, 32, 48, 64, 80, 96, 128, 256, 512, 1024, 2048, 4096$.

the quartic fits around the minima, which lead to the critical interactions $U_{c,gap}(V)$ listed in Table I. Note that the curves flatten out for increasing $v$, so that it becomes more difficult to determine accurately the minima for $v \to 0.5$.

The comparison with the exact value for $V = 0$ shows that the gap exponent $\gamma_2(U, V)$ provides a fairly accurate estimate for the critical interaction. The same accuracy can be obtained when using the ground-state energy exponent $\gamma_0(U, V)$, as we shall show next.

### B. Ground-state energy

As seen from Eq. (36), the $1/L$ corrections to the ground-state energy density also permit us to locate the Mott transition in the extended $1/r$-Hubbard model, in the same way as with the two-particle gap. In Fig. 11 we show the exponent

TABLE I. Critical interaction strengths for the extended $1/r$-Hubbard model, as obtained from the two-particle gap, the ground-state energy, the Luttinger parameter, and the structure factor for systems with $16 \leqslant L \leqslant 80$ lattice sites. For $V = 0$, the exact result in the thermodynamic limit is known [20], $U_c(V = 0) = 1$.

| $V/U$ | $U_{c,gap}(V)$ | $U_{c,gs}(V)$ | $U_{c,LL}(V)$ | $U_{c,sf}(V)$ | $\overline{U}_c(V)$ |
|---|---|---|---|---|---|
| 0 | 1.009 | 1.000 | 1.033 | 0.965 | 1.002 |
| 0.1 | 1.024 | 1.022 | 1.056 | 0.984 | 1.021 |
| 0.2 | 1.055 | 1.056 | 1.090 | 1.018 | 1.055 |
| 0.3 | 1.109 | 1.116 | 1.144 | 1.075 | 1.111 |
| 0.4 | 1.202 | 1.221 | 1.243 | 1.175 | 1.210 |
| 0.5 | 1.425 | 1.500 | 1.540 | 1.456 | 1.480 |
| 0.6 | 0.828 | 0.838 | 0.883 | 0.876 | 0.856 |
| 0.7 | 0.587 | 0.600 | 0.616 | 0.611 | 0.604 |

$\gamma_0(U, V)$, as obtained from the fit of the finite-size data in the range $16 \leqslant L \leqslant 80$ to the algebraic function in Eq. (35). Also shown in the figure are the quartic fits around the minima, which lead to the critical interactions $U_{c,gs}(V)$ listed in Table I.

The critical interaction strengths obtained from the minima of $\gamma_0(U, V)$ agree very well with the exact result at $V = 0$ and with the values obtained from the gap exponent $\gamma_2(U, V)$ with deviations in the low percentage range. Therefore we can be confident that we found reliable estimates for the critical interaction strength for the Mott transition.

### C. Luttinger parameter

As an alternative way to locate the Mott transition, we monitor the Luttinger parameter and determine $U_c(U, V)$ from the condition [25]

$$K(U_c(V), v) = \tfrac{1}{2} \tag{46}$$

for fixed ratios $v = V/U$; see also Ref. [23].

In Fig. 12 we show the Luttinger parameter $K(L; U, V)$ from DMRG calculations for the extended $1/r$-Hubbard

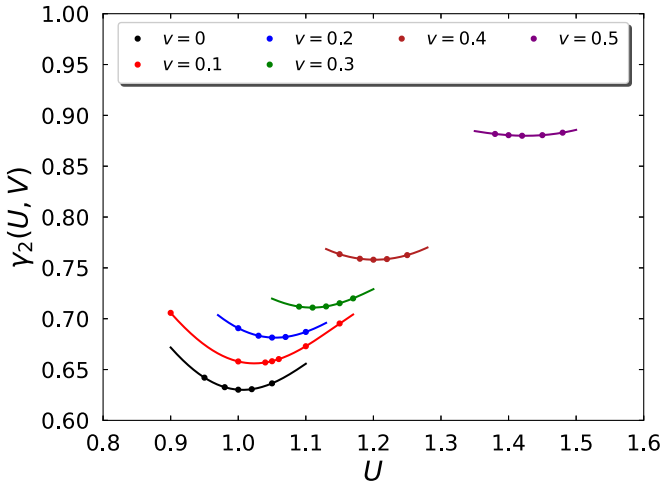


FIG. 10. Exponent $\gamma_2(U, V)$ for the two-particle gap in the extended $1/r$-Hubbard model as a function of $U$ for various values of $v = V/U$, based on system sizes $16 \leqslant L \leqslant 80$. The minimum of the curve determines $U_{c,gap}(V)$.

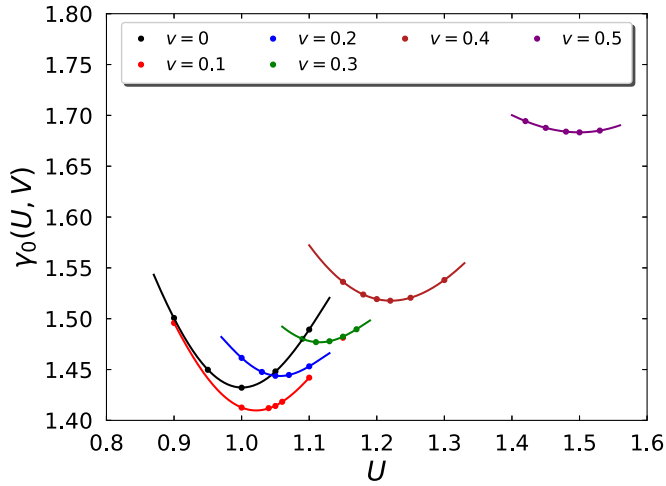


FIG. 11. Exponent $\gamma_0(U, V)$ for the ground-state energy of the extended $1/r$-Hubbard model as a function of $U$ for various values of $v = V/U$, based on system sizes $16 \leqslant L \leqslant 80$. The minimum of the curve determines $U_{c,gs}(V)$.

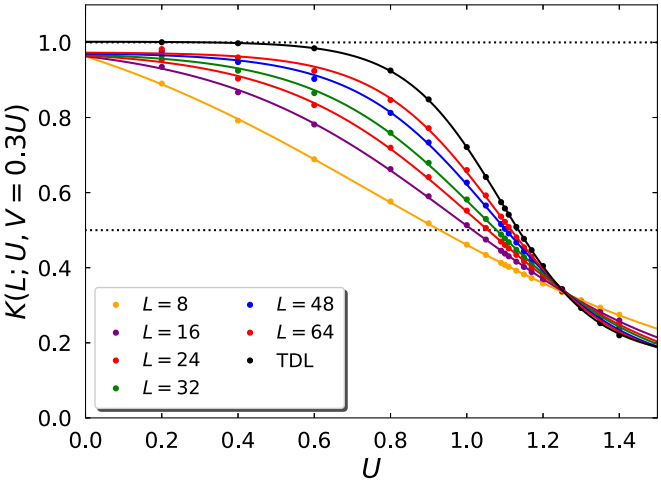


FIG. 12. Luttinger parameter $K(L;U,V)$ from DMRG calculations for the extended $1/r$-Hubbard model with nearest-neighbor interaction $V=0.3U$ as a function of $U$ for system sizes $L=8,16,24,32,48,64$ including a second-order polynomial extrapolation to the thermodynamic limit (TDL). The intersection of the extrapolation with $K_c=1/2$ determines $U_c(V)$.

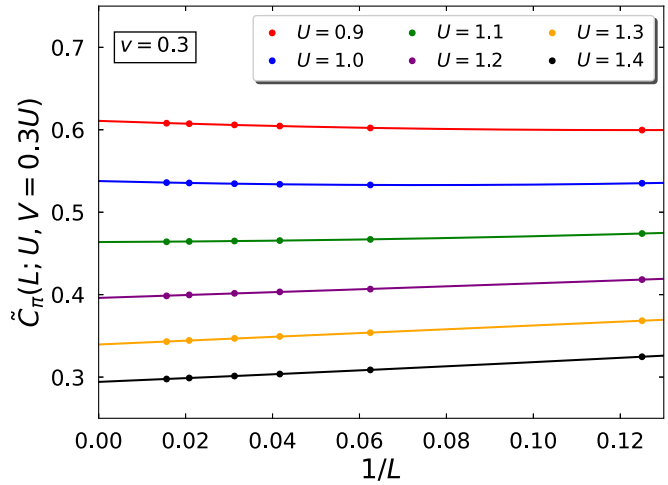


FIG. 13. Structure factor $\tilde{C}_\pi(L;U,V)$ at $q=\pi$ as a function of $1/L$ for various values of $U$ for the extended $1/r$-Hubbard model with nearest-neighbor interaction $V=0.3U$ for system sizes $L=8,16,24,32,48,64$. Curves are second-order polynomial extrapolations to the thermodynamic limit; see Eq. (48).

model with nearest-neighbor interaction $V=0.3U$ as a function of $U$ for system sizes $L=8,16,24,32,48,64$ including a second-order polynomial extrapolation to the thermodynamic limit. The intersection of the extrapolation into the thermodynamic limit with $K_c=1/2$ determines $U_c(V)$. To obtain a reliable estimate for the intersection, either we can use the two data points closest to the transition and perform a linear interpolation, in this case $U=1.1$ and $U=1.2$, or, alternatively, we use a four-parameter fit of the whole data set that employs the information that the Luttinger parameter deviates from unity by exponentially small terms for $U,V\to 0$,

$$K(U,V)=a+b\tanh(c+dU) \tag{47}$$

to fit the extrapolated data for finite values of $U$ to a continuous curve which is parametrized by $a,b,c,d$ that depend on $v$. Then, we solve Eq. (46) for $U_{c,LL}(V)$. The results are also listed in Table I.

Alternatively, we could have solved Eq. (46) for each system size and extrapolated the resulting system-size-dependent critical interaction strengths to the thermodynamic limit. Since the results deviate more strongly from the exact value for $V=0$, we refrain from pursuing this approach further.

As seen from Table I, the critical values from the Luttinger parameter systematically overestimate the correct interaction strengths by some 3%. A similar effect was found for the charge-density-wave transition in a one-dimensional model for spinless fermions with nearest-neighbor interactions (the "$t$-$V$ model") [26]. Apparently, much larger systems are required to overcome this systematic error. We do not apply correction factors for a better fit, but use the critical interaction strengths $U_{c,LL}(V)$ as an upper bound to the exact value $U_c(V)$.

### D. Structure factor and CDW order parameter

For the $1/r$-Hubbard model, the finite-size corrections to the structure factor $\tilde{C}_\pi(U,V)\equiv\tilde{C}(\pi;U,V)$,

$$\tilde{C}_\pi(L;U,V)=\tilde{C}_\pi(U,V)+\frac{C_1(U,V)}{L}+\frac{C_2(U,V)}{L^2}, \tag{48}$$

and the CDW order parameter $N_\pi(L;U,V)$ [see Eq. (44)] permit us to locate the critical interaction strength. In Fig. 13 we show the structure factor for $v=0.3$ and various values of $U$ as a function of inverse system size for $L=8,16,24,32,48,64$.

As can be seen from the figure, the coefficient in $1/L$ changes its sign at the critical interaction strength,

$$C_1(U_{c,sf}(V),V)=0. \tag{49}$$

To see this more clearly, in Fig. 14(a) we show the coefficient $C_1(U,V)$ as a function of $U$ for $v=0.1$, $v=0.3$, and $v=0.5$ and fit the data to a Fano resonance,

$$C_1^{\text{Fano}}(U,V)=a(V)+b(V)\frac{[q_F(V)\Gamma(V)+U-U_c(V)]^2}{[\Gamma(V)]^2+[U-U_c(V)]^2}. \tag{50}$$

Analogously, we find the critical interaction strengths in the CDW phase from the $1/L$ corrections to the CDW order parameter (29) [see Eq. (44)] in Fig. 14(b).

As in our study of the $1/r$-Hubbard model [23], a bound state that interacts with the continuum shows up in physical quantities and thus contributes a Fano resonance to various physical quantities, with weight of the order $1/L$. Using the Fano resonance formula and the conditions $C_1(U_{c,sf},V)=0=N_1(U_{c,sf},V)$, the $1/L$ corrections of the structure factor and the CDW order parameter provide the estimate $U_{c,sf}(V)$ for the critical interaction. The resulting data are listed for various $v$ in Table I.

The critical interaction strength $U_{c,sf}(V)$ systematically underestimates the exact value for the Mott transition by a few percent. Together with the critical interaction strength from

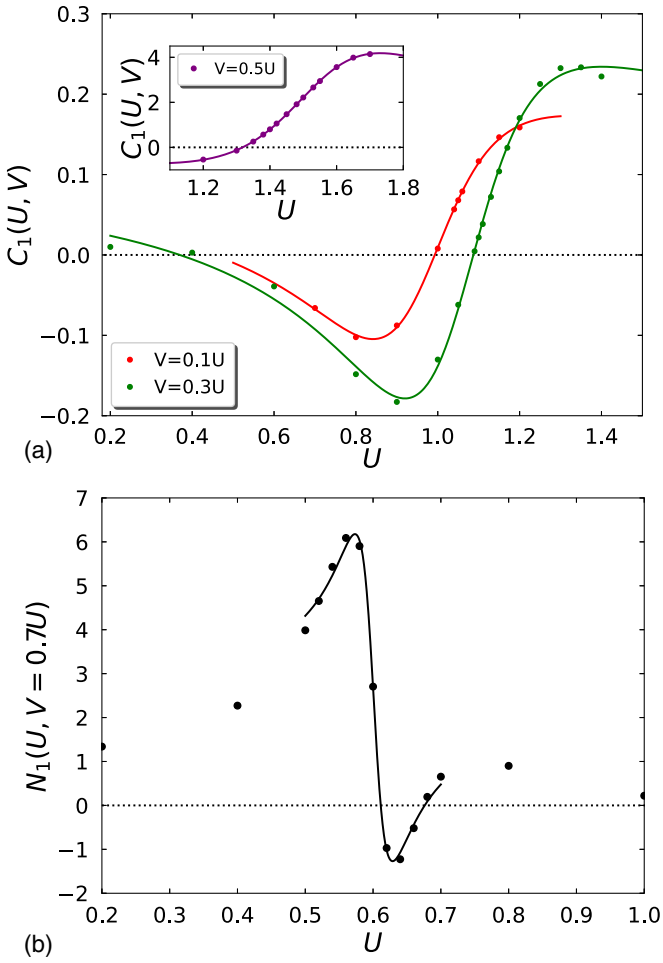


FIG. 14. (a) Finite-size coefficient $C_1(U,V)$ of the structure factor as a function of $U$ for the extended $1/r$-Hubbard model for $v = 0.1$ and $v = 0.3$ (inset: $v = 0.5$). (b) Finite-size coefficient $N_1(U, V = 0.7U)$ for the CDW order parameter; see Eqs. (29) and (44). Curves are fitted Fano resonance curves; see Eq. (50).

the Luttinger parameter $U_{c,LL}(V)$, we thus can set tight limits to $U_c(V)$.

### E. Critical interactions for fixed interaction ratios

In Table I we collect the results for the critical interaction strengths $U_c(V)$ obtained from the analysis of the two-particle gap, the ground-state energy, the Luttinger parameter, and the structure factor for $v = V/U = 0, 0.1, 0.2, 0.3, 0.4, 0.5, 0.6, 0.7$, as obtained from Secs. IV A–IV D. We observe the following.

(i) The arithmetic average of the four values, $\overline{U}_c$, reproduces the exact result at $V = 0$ with an accuracy of a few per mille.

(ii) The values for $U_{c,gs}(V)$ are close to the average for all $V$, with a deviation below 2%. Therefore the ground-state exponent alone provides a reliable estimate for $U_c(V)$ in all cases.

(iii) The estimates $U_{c,LL}(V)$, using the Luttinger parameter, and $U_{c,sf}$, using the structure factor, systematically overestimate and underestimate, respectively, the critical interaction strength for the transition from the Luttinger liquid to the Mott-Hubbard insulator. Therefore they provide natural bounds to $U_c(V)$ for $v \leqslant 0.5$.

(iv) The transitions to the CDW insulator at $v = 0.6, 0.7$ can be determined fairly accurately from all four approaches individually.

In Fig. 1, we connect the data points for $\overline{U}_c(V)$ using a third-order spline interpolation. Error bars at the data points result from the overestimates and underestimates listed in Table I. In Fig. 1 we also include the results from the analysis for the Mott transition between the Luttinger liquid and the CDW insulator at fixed $U = 0.2$, as we discuss next.

### F. Transitions at fixed Hubbard interaction

Lastly, we study the metal-to-insulator transition at fixed Hubbard interaction $U$ as a function of $V$, namely for $U = 0.2$ and $U = 1.7$.

#### *1. Transition from Luttinger liquid to CDW insulator*

At $U = 0.2$, we find a transition from the Luttinger liquid metal to the CDW insulator at $V_c(U = 0.2) = 0.29 \pm 0.01$. The analysis follows the route outlined in Secs. IV A–IV E and will not be repeated here. We increase $V$ in steps of $\Delta V = 0.02$ around the transition.

Using the coefficient $\gamma_0$ from the ground-state energy (see Sec. IV B), we find $V_{c,gs}(U = 0.2) = 0.286$; the coefficient $\gamma_2$ from the two-particle gap in Sec. IV A leads to $V_{c,gap}(U = 0.2) = 0.280$; and the Luttinger parameter of Sec. IV C leads to $V_{c,LL}(U = 0.2) = 0.298$, almost identical to the values from the structure factor (see Sec. IV D). This leads to the average value quoted above.

Due to the absence of perfect nesting in the dispersion relation, it requires a finite interaction strength $V$ to stabilize the CDW phase even at $U = 0$. Qualitatively, Hartree-Fock theory leads to the same result. Hartree-Fock theory systematically overestimates the stability of the CDW phase and thus underestimates $V_c(U)$; see Fig. 1. The analytical approach can be improved by including second-order corrections to Hartree-Fock theory; see, e.g., Refs. [26,33]. This is beyond the purpose of our present analysis.

#### *2. Transition from Mott-Hubbard to CDW insulator*

At $U = 1.7$, not included in the phase diagram in Fig. 1, we have a brief look at the transition from the Mott-Hubbard insulator to the CDW insulator. The results for the two-particle gap are shown in Fig. 15. They are corroborated by the behavior of the order parameter quantities $C_\pi$ and $N_\pi$. The analysis of the parameters $\gamma_0$ and $\gamma_2$ leads to quantitatively identical but less accurate results.

For the one-dimensional extended Hubbard model it is known that the critical interaction is larger than $U/2$. For the extended $1/r$-Hubbard model we also find $V_c = 0.87 \pm 0.01 > 1.7/2 = 0.85$ for the onset of the CDW. When expressed in units of the bandwidth, the offset of $\delta_c(U) = V_c(U) - U/2$ agrees almost quantitatively with the value obtained from DMRG and QMC calculations for the one-dimensional extended Hubbard model, $\delta_c(U = 1.7) \approx 0.02$; see Ref. [34].

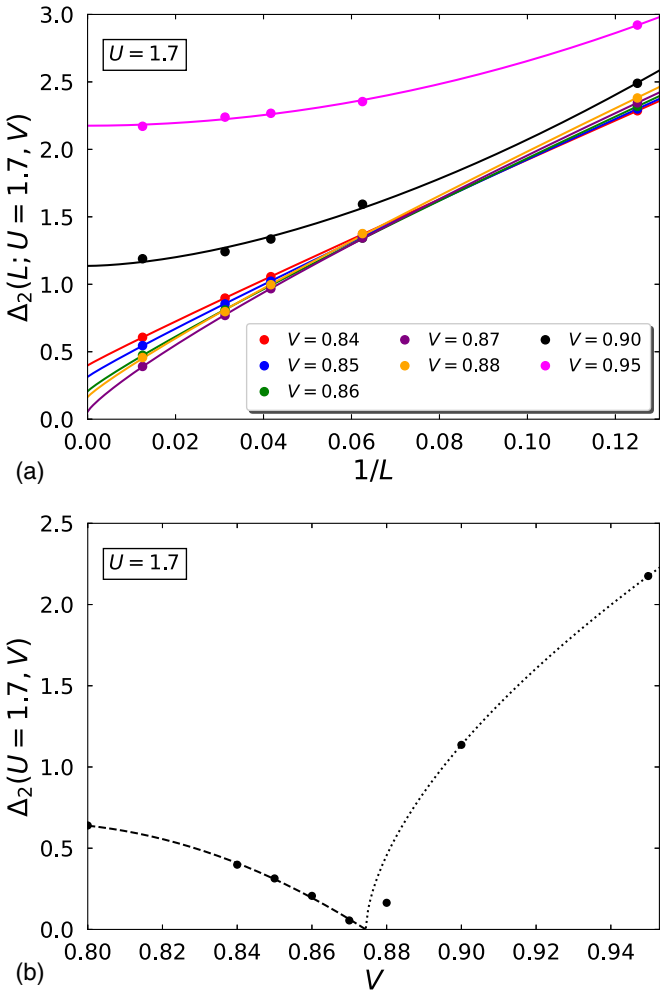


FIG. 15. (a) Two-particle gap for the extended $1/r$-Hubbard model at $U = 1.7$ for various values of $V$ as a function of $1/L$ for $L = 8, 16, 32, 64, 80$. (b) Extrapolated two-particle gap as a function of $V$.

The shift $\delta_c(U)$ can be determined analytically using higher-order strong-coupling perturbation [35]. Unfortunately, this program cannot be carried out for the extended $1/r$-Hubbard model because the exact ground state is not known for the effective spin model which is a linear combination of the Heisenberg model with nearest-neighbor interaction and the Haldane-Shastry model with $1/r^2$ exchange interaction [36,37]. A variational strong-coupling approach that employs the Baeriswyl wave function [38,39] cannot be carried out analytically either because it requires the evaluation of $\langle \hat{T}^3 \rangle$ in the Gutzwiller-projected Fermi sea.

In the one-dimensional extended Hubbard model, there is a bond-order-wave phase below a critical interaction strength $U_{\rm tri}$ that separates the Mott-Hubbard and CDW insulators [16–18]. For $U > U_{\rm tri}$, the transition from the Mott-Hubbard insulator to the CDW insulator is discontinuous. As can be seen from Fig. 15, we also find indications for the existence of a bond-order-wave phase. The charge gap of the Mott-Hubbard insulator closes around $V_c(U = 1.7) \approx 0.87$ and reopens beyond $V_c(U = 1.7)$ with a small value. The extrapolation of the gap remains linear as a function of $1/L$ even at $V = 0.88$, as seen in Fig. 15(a). For larger values of $V$, the gap drastically increases, and the extrapolation displays a $1/L^2$ behavior for large $L$. The same behavior of the gap was observed for the one-dimensional extended Hubbard model at $U = 2W$ [17,18], where it was numerically shown in detail that as a function of $V$ the Mott-Hubbard insulator turns into a bond-order-wave insulator before the CDW phase eventually takes over.

Further investigations are necessary to corroborate the existence of a bond-order-wave phase in the vicinity of the CDW transition also for the extended $1/r$-Hubbard model. Note, however, that we do not expect a bond-order wave as an intermediate phase for small interactions because in the extended $1/r$-Hubbard model the metallic Luttinger liquid overrides a conceivable bond-order wave.

## V. CONCLUSIONS

In this paper we applied the density-matrix renormalization group (DMRG) method to the half-filled extended $1/r$-Hubbard model where the decay of the electron transfer amplitudes is proportional to the inverse chord distance of two lattice sites on a ring. The model describes a linear dispersion within the Brillouin zone and thus provides an ideal case to study the Mott-Hubbard transition because it lacks Umklapp scattering. Therefore the metal-to-insulator transitions occur at finite interaction strengths. Consequently, all generic phases, namely Luttinger liquid metal, Mott-Hubbard insulator, and charge-density-wave insulator, occupy a finite region in the $(U, V)$ ground-state phase diagram; see Fig. 1.

Mapping the quantum phase transition boundaries for the specific model is one of the main achievements of this work. To this end, we use DMRG data for up to $L = 80$ sites to calculate the ground-state energy, the two-particle gap, the momentum distribution, the Luttinger parameter, and the structure factor. The finite-size behavior of the ground-state energy, of the two-particle gap, and of the structure factor permit us to determine the critical interaction parameters for the instability of the Luttinger liquid metal, which turns into the Mott-Hubbard insulator and the charge-density-wave insulator, respectively. Moreover, we monitor the Luttinger parameter, which also signals the breakdown of the Luttinger liquid metal at a metal-to-insulator transition. We tested the validity of our analysis against exact results for $V = 0$, for which analytic results for the ground-state energy and the gap exist for all interactions $U$ and system sizes $L$.

The phase diagram in Fig. 1 shows that the nearest-neighbor interaction and the Hubbard interaction counteract each other. On the one hand, the Mott transition shifts to larger values; that is, a weak-to-moderate nearest-neighbor interaction stabilizes the Luttinger liquid metal. Apparently, the two-particle scattering interaction becomes smoother in position space and renders the total interaction less effective. On the other hand, as can readily be understood from classical considerations, the Hubbard interaction opposes the formation of a charge-density wave because, by definition, a CDW augments the particle density on the same lattice site.

In contrast to the "standard" extended Hubbard model in one dimension, the absence of Umklapp scattering and the competition of both interactions leads to an extended

metallic region in the phase diagram. The extrapolations suggest that there is a tricritical point where all three phases touch. It will be interesting to analyze this region in phase space with higher accuracy, i.e., more data points in the $(U, V)$ parameter space close to $(U_{\text{tri}}, V_{\text{tri}}) \approx (1.5, 0.75)$, and larger system sizes, $L > 80$. Moreover, a conceivable bond-order wave above the tricritical point between the Mott insulator and charge-density-wave insulator should be investigated in more detail. These tasks are left for future studies.

## ACKNOWLEDGMENTS

Ö.L. has been supported by the Hungarian National Research, Development, and Innovation Office (NKFIH) through Grant No. K134983 and by TKP2021-NVA by the Quantum Information National Laboratory of Hungary. Ö.L. also acknowledges financial support from the Hans Fischer Senior Fellowship program funded by the Technical University of Munich Institute for Advanced Study and from the Center for Scalable and Predictive Methods for Excitation and Correlated Phenomena (SPEC), which is funded as part of the Computational Chemical Sciences Program by the U.S. Department of Energy (DOE), Office of Science, Office of Basic Energy Sciences, Division of Chemical Sciences, Geosciences, and Biosciences, at Pacific Northwest National Laboratory.

## APPENDIX: HARTREE-FOCK THEORY

### 1. CDW Hartree-Fock Hamiltonian

In Hartree-Fock theory, we decouple the two-particle interaction as follows:

$$\hat{D}^{\text{HF}} = \hat{D}^{\text{H}} = \sum_l \langle \hat{n}_{l,\uparrow}\rangle \hat{n}_{l,\downarrow} + \hat{n}_{l,\uparrow}\langle \hat{n}_{l,\downarrow}\rangle - \langle \hat{n}_{l,\uparrow}\rangle\langle \hat{n}_{l,\downarrow}\rangle, \tag{A1}$$

$$\hat{V}^{\text{HF}} = \hat{V}^{\text{H}} + \hat{V}^{\text{F}}, \tag{A2}$$

$$\hat{V}^{\text{H}} = \sum_l (\langle \hat{n}_l\rangle - 1)(\hat{n}_{l+1} - 1) + (\hat{n}_l - 1)(\langle \hat{n}_{l+1}\rangle - 1) - (\langle \hat{n}_l\rangle - 1)(\langle \hat{n}_{l+1}\rangle - 1), \tag{A3}$$

$$\hat{V}^{\text{F}} = \sum_{l,\sigma} \langle \hat{c}^+_{l,\sigma}\hat{c}_{l+1,\sigma}\rangle \hat{c}_{l,\sigma}\hat{c}^+_{l+1,\sigma} + \hat{c}^+_{l,\sigma}\hat{c}_{l+1,\sigma}\langle \hat{c}_{l,\sigma}\hat{c}^+_{l+1,\sigma}\rangle - \langle \hat{c}^+_{l,\sigma}\hat{c}_{l+1,\sigma}\rangle\langle \hat{c}_{l,\sigma}\hat{c}^+_{l+1,\sigma}\rangle. \tag{A4}$$

Here, where $\langle \hat{A}\rangle$ denotes the ground-state expectation value of the operator $\hat{A}$,

$$\langle \hat{A}\rangle \equiv \langle \Phi_0|\hat{A}|\Phi_0\rangle, \tag{A5}$$

with $|\Phi_0\rangle$ as the ground state of the Hartree-Fock Hamiltonian $\hat{H}^{\text{HF}}$; see below. We make the CDW ansatz for the order parameter

$$\langle \hat{n}_{l,\sigma}\rangle = \tfrac{1}{2}(1 + (-1)^l \Delta) \tag{A6}$$

with the real CDW parameter $\Delta \geqslant 0$ and introduce the abbreviation

$$B = \langle \hat{c}^+_{l,\sigma}\hat{c}_{l+1,\sigma}\rangle = \mathrm{i}b. \tag{A7}$$

Particle-hole symmetry implies that $B$ is purely complex at half band filling, i.e., $b$ is real. Note that we disregard a possible bond-order wave (BOW) by assuming that $B$ does not alternate from site to site.

With these abbreviations, we can rewrite the Hartree-Fock interaction at half band filling as

$$\hat{D}^{\text{H}} = \frac{L}{4}(1 - \Delta^2) + \frac{\Delta}{2}\sum_{l,\sigma}(-1)^l \hat{n}_{l,\sigma}, \tag{A8}$$

$$\hat{V}^{\text{H}} = L\Delta^2 - 2\Delta\sum_{l,\sigma}(-1)^l \hat{n}_{l,\sigma}, \tag{A9}$$

$$\hat{V}^{\text{F}} = 2Lb^2 + \mathrm{i}b\sum_{l,\sigma}[\hat{c}^+_{l,\sigma}\hat{c}_{l+1,\sigma} - \hat{c}^+_{l+1,\sigma}\hat{c}_{l,\sigma}]. \tag{A10}$$

The resulting single-particle problem defines the Hartree-Fock Hamiltonian for a possible CDW ground state

$$\hat{H}^{\text{HF}} = \hat{T} + U\hat{D}^{\text{H}} + V(\hat{V}^{\text{H}} + \hat{V}^{\text{F}}). \tag{A11}$$

It has to be solved self-consistently; that is, $\Delta$ must be chosen such that the ground state fulfills Eq. (A6).

### 2. Diagonalization of the Hartree-Fock Hamiltonian

In the CDW phase, the Hartree-Fock Hamiltonian is identical for both spin species, $\hat{H}^{\text{HF}} = \sum_\sigma \hat{H}^{\text{HF}}_\sigma$. Dropping the spin index, we must diagonalize

$$\hat{H}_{\text{sf}} = \sum_k \epsilon(k)\hat{C}^+_k\hat{C}_k + \left(\frac{U}{2} - 2V\right)\Delta\sum_l(-1)^l\hat{n}_l + \mathrm{i}b\sum_l[\hat{c}^+_l\hat{c}_{l+1} - \hat{c}^+_{l+1}\hat{c}_l] + C \tag{A12}$$

for spinless fermions ("sf"), where $C = UL/8(1 - \Delta^2) + LV\Delta^2/2 + LVb^2$. In momentum space, the Hamiltonian reads

$$\hat{H}_{\text{sf}} = C + {\sum_k}' [(\epsilon(k) + b(k))\hat{C}^+_k\hat{C}_k + (\epsilon(k+\pi) - b(k))\hat{C}^+_{k+\pi}\hat{C}_{k+\pi}] + \left(\frac{U}{2} - 2V\right)\Delta{\sum_k}'(\hat{C}^+_k\hat{C}_{k+\pi} - \hat{C}^+_{k+\pi}\hat{C}_k), \tag{A13}$$

where the prime on the sum indicates the $k$-space region $-\pi < k < 0$ and $b(k) = -2bV\sin(k) \geqslant 0$.

We diagonalize $\hat{H}_{\text{sf}}$ with the help of the linear transformation

$$\hat{C}_k = c_k\hat{\alpha}_k - s_k\hat{\beta}_k,$$
$$\hat{C}_{k+\pi} = s_k\hat{\alpha}_k + c_k\hat{\beta}_k, \tag{A14}$$

where we abbreviate $c_k \equiv \cos(\varphi_k)$ and $s_k = \sin(\varphi_k)$. The mixed terms in $\hat{H}_{\text{sf}}$ vanish when we demand

$$\tan(2\varphi_k) = -\frac{(2V - U/2)\Delta}{b(k) + (\epsilon(k) + \epsilon(k+\pi))/2} \geqslant 0. \tag{A15}$$

The diagonal terms result in

$$\hat{H}_{\text{sf}} = {\sum_k}' E_\alpha(k)\hat{\alpha}^+_k\hat{\alpha}_k + E_\beta(k)\hat{\beta}^+_k\hat{\beta}_k + C \tag{A16}$$

for the Hartree-Fock quasiparticle Hamiltonian, and we obtain

$$E_\alpha(k) = \tfrac{1}{2}(\epsilon(k) + \epsilon(k+\pi)) - s(k),$$
$$E_\beta(k) = \tfrac{1}{2}(\epsilon(k) + \epsilon(k+\pi)) + s(k) \tag{A17}$$

for the dispersion relations for the lower and upper quasiparticle bands, where

$$s(k) = \sqrt{\left[2V - \frac{U}{2}\right]^2 \Delta^2 + \left[b(k) + \frac{\epsilon(k) - \epsilon(k+\pi)}{2}\right]^2} \tag{A18}$$

is positive so that $E_\alpha(k) < E_\beta(k)$ for all $-\pi < k < 0$. Therefore the ground state contains only $\alpha$ particles,

$$|\Phi_0\rangle = \prod_{-\pi<k<0,\sigma} \hat{\alpha}^+_{k,\sigma}|\text{vac}\rangle, \tag{A19}$$

where we reintroduced the spin index.

### 3. Self-consistency equations and CDW transition

The self-consistency equations (A6) and (A7) become

$$\Delta = \Delta \int_{-\pi}^{0} \frac{dk}{\pi} \frac{2V - U/2}{s(k)} \tag{A20}$$

and

$$b = -\int_{-\pi}^{0} \frac{dk}{2\pi} \frac{\sin(k)[b(k) + (\epsilon(k) - \epsilon(k+\pi))/2]}{s(k)}$$

in the thermodynamic limit. The set $\{\Delta = 0, b = -1/\pi\}$ provides the solution for noninteracting particles.

Within Hartree-Fock theory, the CDW transition is continuous. We seek a solution for $\Delta = 0^+$ and $b = -1/\pi$ so that $V_c(U)$ must obey the equation

$$\frac{1}{2V_c(U) - U/2} = \int_0^\pi \frac{dk}{\pi} \frac{1}{1/4 + 2V_c(U)\sin(k)/\pi}. \tag{A21}$$

Using MATHEMATICA [40], and with the abbreviation $a_c = 8V_c/\pi$, we find

$$\frac{1}{a_c - 2U/\pi} = \frac{\pi}{\sqrt{1-a_c^2}} - \frac{2}{\sqrt{1-a_c^2}} \arctan\left(\frac{a_c}{\sqrt{1-a_c^2}}\right). \tag{A22}$$

This equation must be solved numerically for given $U$. The resulting curve $V_c^{\text{HF}}(U)$ is shown in Fig. 1.


[1] N. F. Mott, *Metal-Insulator Transitions*, 2nd ed. (Taylor & Francis, London, 1990).

[2] F. Gebhard, *The Mott Metal-Insulator Transition*, Springer Tracts in Modern Physics, Vol. 137 (Springer, Berlin, 1997).

[3] We denote all transitions that are driven by the electron-electron interaction as "Mott transitions." Subclasses comprise the Mott-Hubbard transition, which requires no symmetry breaking, and the charge-density-wave (CDW) transition, where the gap is the consequence of a symmetry breaking.

[4] J. Hubbard, Electron correlations in narrow energy bands, Proc. R. Soc. A **276**, 238 (1963).

[5] M. Gutzwiller, Effect of correlation on the ferromagnetism of transition metals, Phys. Rev. Lett. **10**, 159 (1963).

[6] J. Kanamori, Electron correlation and ferromagnetism of transition metals, Prog. Theor. Phys. **30**, 275 (1963).

[7] N. F. Mott, The basis of the electron theory of metals, with special reference to the transition metals, Proc. Phys. Soc. A **62**, 416 (1949).

[8] E. H. Lieb and F. Y. Wu, Absence of Mott transition in an exact solution of the short-range, one-band model in one dimension, Phys. Rev. Lett. **21**, 192 (1968).

[9] F. Essler, H. Frahm, F. Göhmann, A. Klümper, and V. Korepin, *The One-Dimensional Hubbard Model* (Cambridge University Press, Cambridge, 2010).

[10] S. R. White and R. M. Noack, Real-space quantum renormalization groups, Phys. Rev. Lett. **68**, 3487 (1992).

[11] S. R. White, Density matrix formulation for quantum renormalization groups, Phys. Rev. Lett. **69**, 2863 (1992).

[12] S. R. White, Density-matrix algorithms for quantum renormalization groups, Phys. Rev. B **48**, 10345 (1993).

[13] U. Schollwöck, The density-matrix renormalization group, Rev. Mod. Phys. **77**, 259 (2005).

[14] R. M. Noack and S. R. Manmana, Diagonalization- and numerical renormalization-group-based methods for interacting quantum systems, AIP Conf. Proc. **789**, 93 (2005).

[15] T. Giamarchi, *Quantum Physics in One Dimension*, International Series of Monographs on Physics (Clarendon, Oxford, 2004).

[16] E. Jeckelmann, Ground-state phase diagram of a half-filled one-dimensional extended Hubbard model, Phys. Rev. Lett. **89**, 236401 (2002).

[17] S. Ejima and S. Nishimoto, Phase diagram of the one-dimensional half-filled extended Hubbard model, Phys. Rev. Lett. **99**, 216403 (2007).

[18] C. Mund, Ö. Legeza, and R. M. Noack, Quantum information analysis of the phase diagram of the half-filled extended Hubbard model, Phys. Rev. B **79**, 245130 (2009).

[19] M. Hohenadler and H. Fehske, Density waves in strongly correlated quantum chains, Eur. Phys. J. B **91**, 204 (2018).

[20] F. Gebhard and A. E. Ruckenstein, Exact results for a Hubbard chain with long-range hopping, Phys. Rev. Lett. **68**, 244 (1992).

[21] F. Gebhard, A. Girndt, and A. E. Ruckenstein, Charge- and spin-gap formation in exactly solvable Hubbard chains with long-range hopping, Phys. Rev. B **49**, 10926 (1994).

[22] P.-A. Bares and F. Gebhard, Asymptotic Bethe-ansatz results for a Hubbard chain with 1/sinh-hopping, Europhys. Lett. **29**, 573 (1995).

[23] F. Gebhard and Ö. Legeza, Tracing the Mott-Hubbard transition in one-dimensional Hubbard models without Umklapp scattering, Phys. Rev. B **104**, 245118 (2021).

[24] A. Georges, G. Kotliar, W. Krauth, and M. J. Rozenberg, Dynamical mean-field theory of strongly correlated fermion systems and the limit of infinite dimensions, Rev. Mod. Phys. **68**, 13 (1996).

[25] T. Giamarchi, *Quantum Physics in One Dimension* (Clarendon, Oxford, 2004).

[26] F. Gebhard, K. Bauerbach, and O. Legeza, Accurate localization of Kosterlitz-Thouless-type quantum phase transitions for one-dimensional spinless fermions, Phys. Rev. B **106**, 205133 (2022).

[27] H. J. Schulz, Correlation exponents and the metal-insulator transition in the one-dimensional Hubbard model, Phys. Rev. Lett. **64**, 2831 (1990).

[28] T. Giamarchi and H. J. Schulz, Correlation functions of one-dimensional quantum systems, Phys. Rev. B **39**, 4620 (1989).

[29] S. Ejima, F. Gebhard, and S. Nishimoto, Tomonaga-Luttinger parameters for doped Mott insulators, Europhys. Lett. **70**, 492 (2005).

[30] S. Szalay, M. Pfeffer, V. Murg, G. Barcza, F. Verstraete, R. Schneider, and Ö. Legeza, Tensor product methods and entanglement optimization for *ab initio* quantum chemistry, Int. J. Quantum Chem. **115**, 1342 (2015).

[31] Ö. Legeza, J. Röder, and B. A. Hess, Controlling the accuracy of the density-matrix renormalization-group method: The dynamical block state selection approach, Phys. Rev. B **67**, 125114 (2003).

[32] Ö. Legeza and J. Sólyom, Quantum data compression, quantum information generation, and the density-matrix renormalization-group method, Phys. Rev. B **70**, 205118 (2004).

[33] P. G. J. van Dongen, Extended Hubbard model at weak coupling, Phys. Rev. B **50**, 14016 (1994).

[34] E. Jeckelmann, Comment on "Accurate ground-state phase diagram of the one-dimensional extended Hubbard model at half filling", Phys. Rev. B **71**, 197101 (2005).

[35] P. G. J. van Dongen, Extended Hubbard model at strong coupling, Phys. Rev. B **49**, 7904 (1994).

[36] F. D. M. Haldane, Exact Jastrow-Gutzwiller resonating-valence-bond ground state of the spin-1/2 antiferromagnetic Heisenberg chain with $1/r^2$ exchange, Phys. Rev. Lett. **60**, 635 (1988).

[37] B. S. Shastry, Exact solution of an $S = 1/2$ Heisenberg antiferromagnetic chain with long-ranged interactions, Phys. Rev. Lett. **60**, 639 (1988).

[38] F. Gebhard and A. Girndt, Comparison of variational approaches for the exactly solvable $1/r$-Hubbard chain, Z. Phys. B **93**, 455 (1994).

[39] M. Dzierzawa, D. Baeriswyl, and M. Di Stasio, Variational wave functions for the Mott transition: The $1/r$ Hubbard chain, Phys. Rev. B **51**, 1993 (1995).

[40] Wolfram Research, Inc., *Mathematica, version 12*, Champaign, IL, 2021.